Accepted Manuscript
Version of Record at: https://doi.org/10.1021/acsaom.3c00067

The Role of Semiconductor Nanostructures in Photon Upconversion Applications

Jill M. Cleveland, Tory A. Welsch, D. Bruce Chase, and Matthew F. Doty*

Department of Materials Science and Engineering, University of Delaware, Newark, DE 19716, USA

E-mail: doty@udel.edu

Abstract

Photon upconversion, a process in which multiple low energy photons are absorbed and re-emitted as higher energy photons, has recently received significant attention due to its potential utility across a wide range of optical application. Traditionally, two types of materials have been used for photon upconversion applications - lanthanide-doped nanocrystals and triplet-triplet annihilation molecules. While these systems have demonstrated good upconversion efficiencies, they both suffer from some limitations, particularly in spectral utilization. In this review, we will highlight the ways semiconductor nanocrystals have been integrated into existing upconverison platforms to address their limitations and improve their usability for some specific upconversion applications. Additionally, we will discuss the recent development of upconversion platforms based entirely on semiconductor nanostructures. These systems rely on the size-, shape-, and composition-dependent optical properties of semiconductors to design upconverting materials with the necessary electronic structure for a specific application. We discuss the current status of these hybrid and pure semiconductor-based upconverters and suggest future directions to further improve their upconversion performance.

Accepted Manuscript
Version of Record at: https://doi.org/10.1021/acsaom.3c00067

Keywords

Upconversion, semiconductor, quantum dots, nanoparticles, lanthanide, triplet-triplet annihilation, TTA

1. Introduction

Photon upconversion is an optical process in which the absorption of two or more low-energy photons results in the emission of a higher-energy photon. The idea of photon upconversion was initially proposed by Bloembergen in 1959 for use in an infrared quantum counter detector.[1] Development of the laser in 1960 allowed experimental realization of photon upconversion and other anti-Stokes processes such as second harmonic generation (SHG). F. Auzel first demonstrated energy transfer upconversion in rare-earth doped crystals in 1966, but significant advances in upconversion have only been realized in the past few decades as a result of rapid developments in the field of nanotechnology.[2] Photon upconverters have been used for a wide range of applications including biomedical imaging,[3,4] therapeutics,[5–7] chemical sensing,[8–10] optoelectronic devices,[11–13] and solar energy harvesting.[14–16]

The performance of upconversion materials can be evaluated using three general metrics.[17] First, upconversion quantum efficiency (UQE) is the probability that a high-energy photon is emitted after absorption of two (or more) low energy photons. UQE is limited by all radiative and non-radiative processes in the material. It is also important to consider the excitation power dependence of the UQE, particularly for UC applications such as solar energy harvesting that require low power excitation. Second, photon energy sacrifice (PES) is the difference in energy between the emitted (high-energy) photon and the combined energy of the absorbed (low-energy) photons. PES arises from the natural relaxation processes that occur in many optical materials. For example, if the sequential absorption of two low-energy photons populates an excited state $E^{'}$ and the system relaxes to an excited state E before emitting a high energy photon, the PES will be given by $E^{'} - E$. Third, absorption

Accepted Manuscript
Version of Record at: https://doi.org/10.1021/acsaom.3c00067

bandwidth (AB) is the spectral range of low-energy photons that can be absorbed by the upconverting material. Closely linked to AB is tunability of the absorption and emission wavelengths. UC platforms based on atomic or molecular species tend to have narrower AB and fixed absorption and emission energies, while platforms based on semiconductor materials will have wider AB and more tunable absorption and emission energies. Which metric is most important depends on the specific application of the upconversion materials being developed, and it is possible to trade these metrics off against one another. For example, PES can be often be intentionally increased in order to suppress competing radiative relaxation processes and maximize UQE.

Two types of materials have been most commonly used for traditional upconversion applications. The first are Lanthanide-doped nanocrystals (Ln-UCs), which undergo excited state absorption or energy transfer upconversion within their unique manifold of 4f electron states. The second are triplet-triplet annihilation molecules (TTAs), which rely on energy transfer between long-lived triplet excited states to generate high-energy photons. Both of these materials have reached relatively high UQEs (on the order of 10% at low excitation fluxes), but they suffer from having limited AB as a direct result of the atomic or molecular nature of the electron energy levels involved in the upconversion process.[18] To combat this problem, Ln-UCs and TTAs can be coupled to a different absorber with a wider AB. Semiconductors tend to have wide absorption bandwidths due to their electronic structure and high density of states, making them an ideal material for this role. In such an application, the semiconductor would be engineered to absorb a wide spectral range of photons and emit photons at the specific wavelength that can be absorbed by the Ln-UCs or TTA upconverter. Semiconductor nanoparticles (or quantum dots, QDs) are of particular interest for this application due to their size-, shape-, and composition-dependent optical properties. In addition to large ABs, QDs have tunable absorption and emission energies ranging from ultraviolet (UV) to the near-infrared (NIR). They also have large absorption coefficients, high photoluminescence quantum yields (PLQY), and exhibit low photobleaching.[19–21] Although hybrid

Accepted Manuscript
Version of Record at: https://doi.org/10.1021/acsaom.3c00067

systems that combine semiconductor absorbers/emitters with Ln-UCs or TTA upconverters partially overcome the limitations of a narrow AB, they still have significant limitations, as described below. For example, the spectrally-downshifted light coming from the semiconductor is typically emitted isotropically, so only a fraction of the downshifted light is absorbed by the Ln-UCs or TTA upconverters. This also introduces additional energy transfer processes and loss pathways that can reduce the overall upconversion efficiency. Moreover, the narrow AB of the Ln-UCs or TTA upconverters means that they can only make use of photons from one region of the solar spectrum, even with a semiconductor sensitizer. This significantly limits their use for solar energy harvesting applications.[17,22]

In this review, we will highlight the role of semiconductor nanoparticles in photon upconversion, both as a component in Ln-UC and TTA systems and as standalone upconversion platform. In section 2 we will briefly define some common upconversion and anti-Stokes processes and identify the relevant mechanisms for this review. In section 3 we discuss Ln-UCs using QDs as both sensitizers and emitters. In section 4 we discuss upconversion in TTAs using QDs as sensitizers. Finally, in section 5 we discuss the development of pure semiconductor-based upconverting material systems.

2. Types of Upconversion Mechanisms

In principle, any anti-Stokes process in which the emitted photon is higher in energy than any absorbed photons can be classified as upconversion. However, the mechanisms behind these processes can vary widely, with significant implications for the potential applications of the upconverting material. Here we will briefly define some of these anti-Stokes optical processes and highlight those which will be relevant in this review.

Second harmonic generation (SHG) is a nonlinear optical process in which two photons with the same frequency combine to produce a photon with twice the frequency, as depicted in Figure 1(a). This process requires simultaneous absorption of two identical photons and

Accepted Manuscript
Version of Record at: https://doi.org/10.1021/acsaom.3c00067

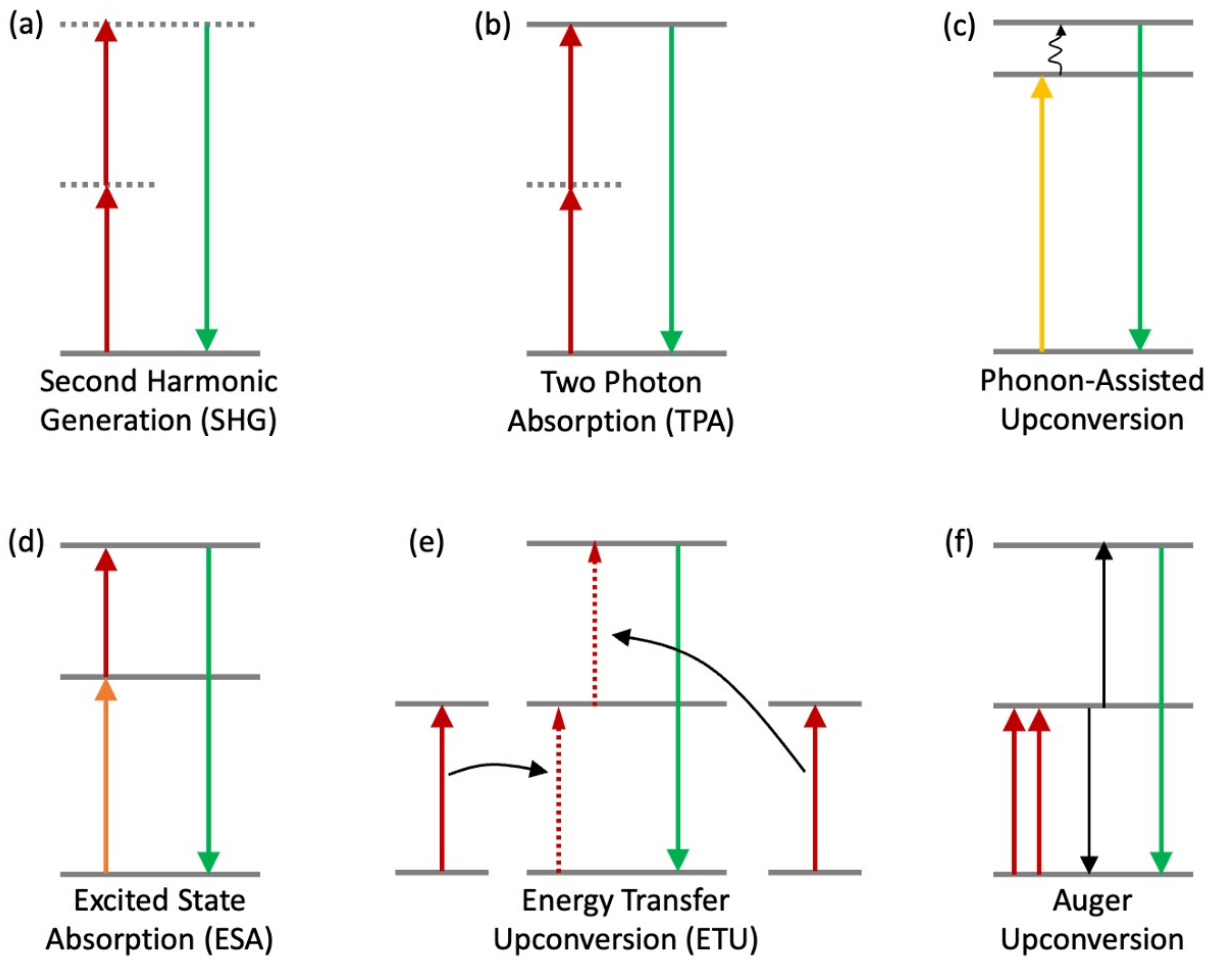

Figure 1: Diagrams of common upconversion mechanisms. (a) SHG - simultaneous absorption of two photons via a virtual intermediate state and virtual excited state. (b) TPA - absorption of two photons via a virtual state to a real excited state. (c) Phonon-assisted UC - absorption of a single photon and phonon(s) to generate anti-Stokes luminescence. (d) ESA - sequential absorption of two photons via a real intermediate state to a real excited state. (e) ETU - energy from absorption of low-energy photons is transferred to generate an emitter in a higher-energy excited state. (f) Auger UC - a biexciton in the intermediate state undergoes Auger recombination to generate a single exciton in the excited state.

occurs via virtual intermediate and excited states. Two photon absorption (TPA) is another nonlinear process in which two photons are absorbed to excite a material via a virtual intermediate state, as depicted in Figure 1(b) Because of the infinitely short lifetime of the virtual intermediate state, both SHG and TPA require very high pump fluence. This limits their potential upconversion applications to situations where high powered lasers can be used as the excitation source. This is rarely the case for imaging, sensing, or solar energy harvesting applications. Phonon-assisted upconversion, as depicted in Figure 1(c), is an anti-Stokes process known to occur in semiconductor QDs due to surface states within the bandgap.[23–26] Excitons are generated in these surface states by absorption of a below-bandgap photon. The carriers are then further promoted by thermal excitation to higher-energy surface states closer to the band edge. Radiative recombination of these carriers results in emission of photons with energy below the material bandgap but above that of the absorbed photon. Phonon-assisted upconversion is unique from the other mechanisms described here in that is only uses one photon rather than two (or more). Because the additional energy is provided by phonons rather than photons, the energy gain is much lower than in other upconversion mechanisms. Due to their limited applications and specific material requirements, SHG, TPA, and phonon-assisted upconversion mechanisms are not included in this review.

The three upconversion mechanisms that are of interest in this article are excited state absorption (ESA), energy transfer upconversion (ETU), and Auger upconversion. These mechanisms are depicted schematically in Figure 1(d-f). All of these mechanisms involve sequential absorption of two (or more) photons via a real intermediate state to generate carriers in a real excited state. ESA is the simplest of the three mechanisms and occurs via a two-step process. First, a low energy photon is absorbed to excite carriers to the intermediate state. Next, a second photon is absorbed to further promote those carriers to the excited state. The carriers undergo radiative relaxation from the excited state back to the ground state, emitting a higher energy photon than either of the absorbed photons in this process.

Accepted Manuscript
Version of Record at: https://doi.org/10.1021/acsaom.3c00067

The key feature in ESA (and what makes it distinct from TPA) is the existence of a real intermediate state, preferably one with a long lifetime. Longer lifetimes of the intermediate state make it more likely that the second photon absorption occurs before the carriers return to the ground state via a radiative or nonradiative process. Radiative recombination of carriers from the intermediate state is typically a major loss pathway in ESA upconversion. The two photons absorbed in ESA do not need to be identical. Depending on the energy of the intermediate state, the two photons can actually be quite different in energy, thus increasing the AB of the material. This is of particular interest in solar energy applications where harvesting a wide range of solar photons is important.

Energy transfer upconversion (ETU), as depicted in Figure 1(e), occurs via an energy transfer process between a sensitizer species and and activator species. Generally, low energy photons are absorbed in the sensitizer. This energy is then transferred to the activator, generating carriers in an excited state. The energy transfer may occur by several mechanisms, including Förster resonance energy transfer (FRET) and triplet-triplet energy transfer (TTET). Subsequent energy transfers from sensitizers to the activator will further promote carriers to higher-energy excited states. Eventually the excited carriers in the activator will relax back to the ground state, releasing high-energy photons. ETU occurs in both Ln-UCs and TTAs and the specifics of those mechanisms will be discussed in subsequent sections. Sometimes, as is the case for some Ln-UCs, the activator alone may undergo upconversion via ESA.

The final upconversion mechanism that will be discussed briefly is Auger upconversion. In Auger upconversion, depicted in Figure 1(f), two excitons are generated in the intermediate state through absorption of two low-energy photons. This pair of excitons then undergoes an Auger recombination process in which the energy released by the recombination of one exciton is transferred to the other, allowing a carrier to be promoted to the excited state. Subsequent radiative recombination from the excited state results in upconversion emission. Auger upconversion often occurs alongside ESA, but has one distinct disadvantage: because

Accepted Manuscript
Version of Record at: https://doi.org/10.1021/acsaom.3c00067

both low-energy photon absorptions are occurring between the ground and intermediate states, materials undergoing Auger upconversion will only absorb a single band of photon energies. In contrast, ESA upconversion can result in absorption of photons from two distinct spectral bands associated with the two different transition energies.

3. Upconversion in Lanthanide-Semiconductor Systems

Upconversion in rare-earth (lanthanide) doped materials has been studied since the 1960s.[2] Lanthanides consist of the group of elements in the periodic table with a partially filled 4f electron shell. In their ionized form, lathanides are typically trivalent with a $4f^N5s^25p^6$ electron configuration, where N = 0-14. This electron configuration gives rise to unique optical properties in lanthanides.[16,27] First, the large number of electron and orbital combinations gives rise to complex energy structures with transition energies across the NIR, VIS, and UV spectral range. Second, the outer 5s and 5p electron shells shield the 4f electrons from crystal-field and vibronic coupling. This results in long excited state lifetimes and electronic transitions that are independent of the surrounding materials. UC has been demonstrated across the entire range of lanthanides.[28]

Generally, a Ln-UC system will consist of three components: a sensitizer, an activator, and a host material. The most commonly studied system is $NaYF_4$:Yb^{3+}/Er^{3+}, which we will use as a representative example to describe Ln-based upconversion. In this system, Yb^{3+} sensitizers and Er^{3+} activators are co-doped in the $NaYF_4$ host nanoparticles. Low energy photons (980nm) are absorbed to promote an electron from the ground $^2F_{7/2}$ state to the excited $^2F_{5/2}$ state, as shown in Figure 2. UC proceeds by an ETU mechanism, whereby energy transfer from the excited Yb^{3+} sensitizer leads to excitation of an Er^{3+} activator via the $^4I_{15/2}$ to $^4I_{11/2}$ transition. Additional low-energy photon absorption in Yb^{3+} followed by energy transfer further excites the Er^{3+} to one of several high-energy states. There are then several possible radiative relaxation pathways for the Er^{3+} activator to return to the

Accepted Manuscript
Version of Record at: https://doi.org/10.1021/acsaom.3c00067

ground state, resulting in upconversion emission in the red or green. Alternatively, when this system is pumped with 1550nm light, upconversion occurs entirely in the Er^{3+} activators via ESA (no sensitizer is required). ESA upconversion in Er^{3+} requires three photon absorption events, compared to only two needed for the Yb^{3+} sensitized ETU process, and the transition energies must very closely match the excitation source energy. ETU has less strict energy matching requirements as phonon-assisted energy transfer can compensate for small energy mismatches. Additionally, Er^{3+} has a smaller absorption cross section than Yb^{3+} ($\sim 10^{-21}$ cm^2 vs $\sim 10^{-20}$ cm^2).[28] Thus, addition of a sensitizer tends to improve UC efficiency, although both (sensitized) ETU and (activator only) ESA may occur in Ln-UC systems.

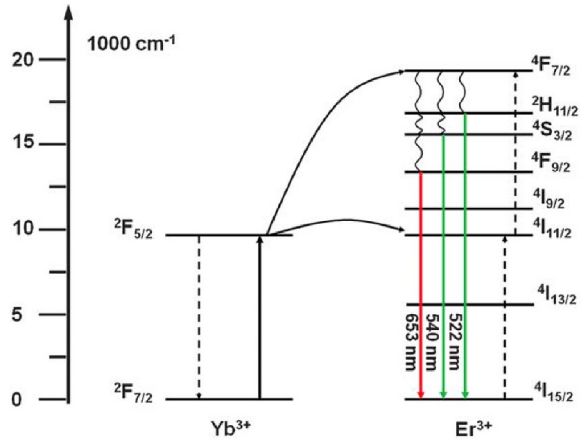

Figure 2: Upconversion mechanism in Yb^{3+}/Er^{3+} Ln-UC system. Absorption of low-energy photons in Yb^{3+} ions and subsequent energy transfer (solid black lines) generate excited state Er^{3+} ions. After phonon relaxation, emission of red or green UCL is possible from several Er^{3+} excited states. Dashed lines show alternative energy pathways. Reproduced with permission from ref 16. Copyright 2011 The Royal Society of Chemistry.

Through over four decades of research, Ln-UC systems have been developed to span a significant range of emission wavelengths, lifetimes, and quantum efficiencies. Despite these advances, the main limitation of Ln-UCs is a small number of available emission and, more importantly, excitation energies. The available energies are limited by the fixed nature of the atomic energy structure.[29] Co-doping multiple types of activator ions can help improve the range of emission energies, but these transitions are still fixed in energy with rather

narrow AB, i.e. they do not achieve a broad spectrum of emission. Excitation energies are even more limited, with most systems requiring either 980nm excitation for Yb^{3+} sensitizers or 808nm excitation for a Nd^{3+}/Yb^{3+} co-sensitized process.[28] Both of these limitations can be addressed by introducing semiconductor nanoparticles as alternate emitters or sensitizers coupled to Ln-UCs.

3.1 Ln-UCs coupled to QD emitters

Ln-UCs can be coupled to QD emitters to improve the range of available emission energies. In this situation, the entire Ln-UC system serves as a sensitizer for the QD emitter. Yan et al. developed a novel nanoheterostructure by coupling CdSe QDs to $NaYF_4$:Yb^{3+}/Er^{3+} nanocrystals.[30] These "CSNY" particles were synthesized via a seeded-growth method that relied on electrostatic attraction between oppositely charged surface ligands to link the two materials. The method resulted in dendritic growth of CdSe QDs on $NaYF_4$:Yb^{3+}/Er^{3+} cores that maintains electronic interactions between the two materials, unlike other methods that relied on silica encapsulation.[31] Illuminating the CSNYs with UV light resulted in a characteristic CdSe emission spectrum centered at 634nm (Figure 3a) and illuminating bare $NaYF_4$:Yb^{3+}/Er^{3+} gave rise to three characteristic Er^{3+} emission bands at 524nm, 542nm, and 660nm (Figure 3b). However, when the full CSNY particles were illuminated with 980nm light, the 524nm and 542nm Er^{3+} emission bands were attenuated by 90% and a new broad peak at 634nm appeared in the spectrum. This result showed efficient energy transfer between the $NaYF_4$:Yb^{3+}/Er^{3+} nanocrystals and the CdSe QDs.

In addition to tuning the emission energy of the Ln-UCs, Yan et al. demonstrated how this type of Ln-QD UC system could be used in optoelectronic devices by creating a NIR photoconductivity switch. CSNY particles were spin-coated onto Si/SiO_2 substrates patterned with Au electrodes and then pretreated with hydrazine to cross-link the QDs. With no illumination, scanning the voltage from -25 to +25 V resulted in negligible current. However, under 980nm illumination, a photocurrent of up to 5 nA was measured, giving an on/off

Accepted Manuscript
Version of Record at: https://doi.org/10.1021/acsaom.3c00067

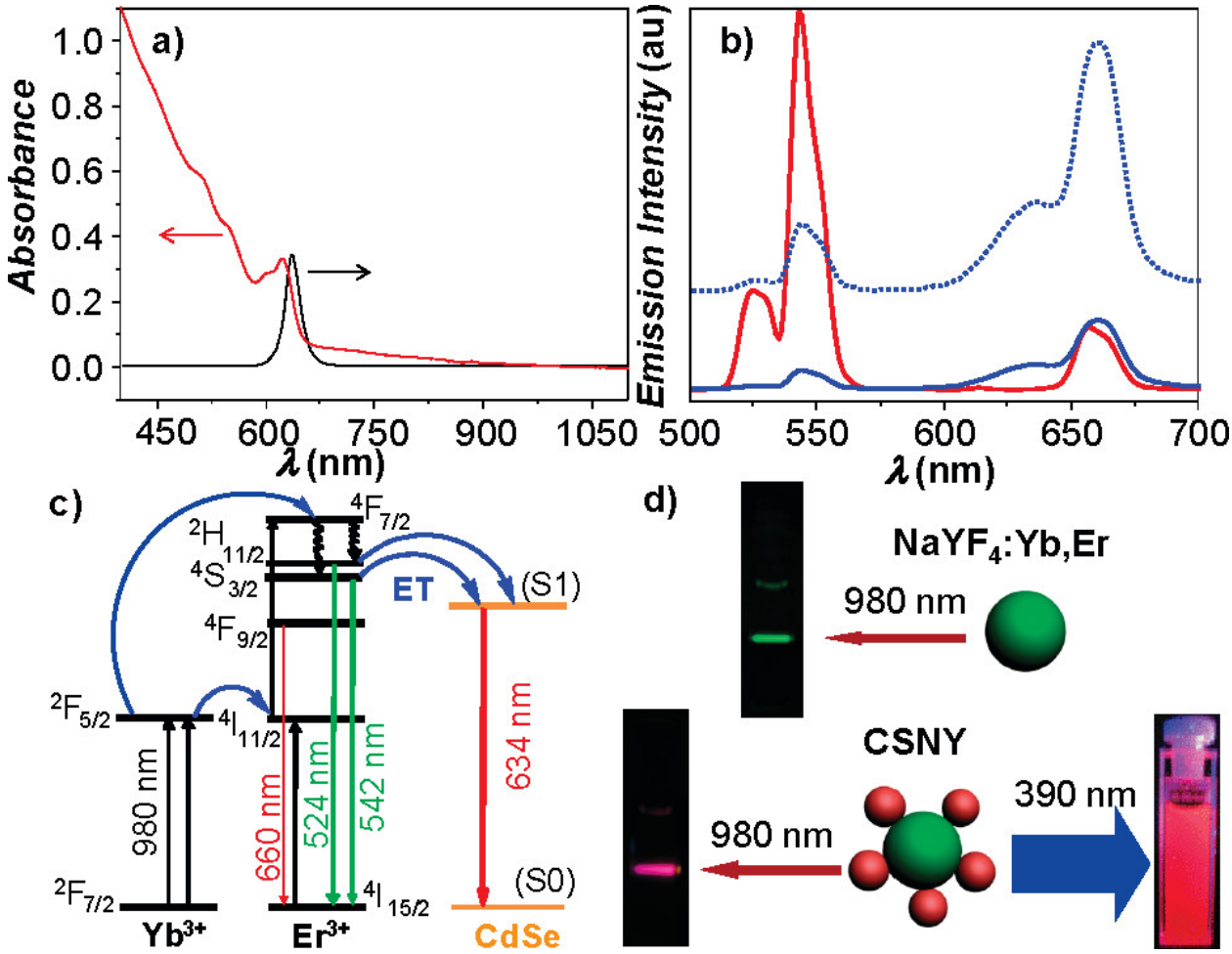

Figure 3: (a) Absorption (red) and PL (black) spectra of CdSe QD-$NaYF_4$:Yb/Er CSNY heterostructure. (b) UC emission spectra of $NaYF_4$:Yb/Er nanocrystals (red) and CSNY (blue). Dashed blue is expansion of solid blue spectrum. (c) Energy level diagram showing UC mechanism in CSNY. (d) Photographs of luminescence from $NaYF_4$:Yb/Er (top) and CSNY (bottom). Reproduced from ref 30. Copyright 2010 American Chemical Society.

ratio of 360. This type of NIR photoconductive behavior is the basis for many upconversion applications in optoelectronic devices, particularly photovoltaics.[16,17,32]

More recently there have been several demonstrations of similar systems in which the CdSe QDs are replaced with perovskite QDs (PeQDs).[33,34] PeQDs have received significant attention in the past decade as a promising material for a variety of optoelectronic applications owing to their remarkable optical properties.[35,36] PeQDs are efficient emitters when pumped with high energy (above bandgap) light in the visible or UV, but cannot be directly excited with NIR pumping. Coupling PeQDs to LnUCs allows indirect excitation of the PeQDs with NIR light. For example, Zheng et al. demonstrated efficient upconversion luminescence (UCL) in $CsPbX_3$ PeQDs (X = Cl, Br, or I) sensitized by $LiYbF_4$:Tm^{3+}@$LiYF_4$ core/shell nanoparticles.[33] In these NPs, absorption of 980nm light by Yb^{3+} ions and subsequent energy transfer to Tm^{3+} ions results in emission peaks in the UV (374 and 362nm), blue (450 and 483nm), red (648nm), and NIR (792nm). UC in this system requires as many as four or five photon absorptions to emit light in the highest energy bands.[28] The UV, blue, and red light emitted from the Ln-UCs can be absorbed by the PeQDs depending on their bandgap. By varying the halide composition in the PeQDs, they were able to achieve full color tuning of the UC luminescence across the visible spectral range. In these systems the primary mechanism is believed to be radiative energy transfer upconversion (RETU), wherein radiative emission from the Ln-UC is is absorbed by the PeQDs and re-emitted following carrier relaxation to the bandedge. A nonradiative FRET mechanism may also contribute, but appears to be less efficient than RETU.[34] RETU is an efficient process for PeQDs due to their large absorption cross section and high PLQY. Moreover, the RETU mechanism made it possible to extend the PL lifetimes of the PeQDs from nanoseconds to milliseconds by varying the Tm^{3+} concentration. These long exciton lifetimes in QD emitters are beneficial for applications such as time-gated PL biosensing because the longer lifetimes can reduce interference from background noise.[33]

Accepted Manuscript
Version of Record at: https://doi.org/10.1021/acsaom.3c00067

3.2 QDs as sensitizers for Ln-UCs

In all of the cases described above, Yb^{3+} was used as the sensitizer because it is the most widely studied and generally the most efficient sensitizer for Ln-UCs. However, there are several limitations of systems relying on Yb^{3+} sensitization. First, Yb^{3+} has a simple electronic structure with a single excited state, resulting in only a single allowed excitation window centered at 980nm.[16] This poses a significant issue for applications such as harvesting below-bandgap photons in photovoltaic devices where the ideal upconverter would harvest a wide range of NIR photons.[37] For some other UC application, such as chemical sensing and bioimaging, a narrow absorption band poses less of an issue. Unfortunately for biological applications, the 980nm absorption of Yb^{3+} overlaps with the absorption of water molecules and can lead to tissue overheating.[7] Finally, while there have been significant improvements to the efficiency of Yb^{3+}-sensitized Ln-UCs, they still suffer from low photoluminescence quantum yields due to the small absorption cross section of Yb^{3+}.[28]

Semiconductor QDs are a promising option for alternative sensitizers in Ln-UC systems due to their high quantum yield, large Stokes shift, and tunable emission energies that overlap with the absorptions of lanthanide ions.[28] When using QDs as sensitizers for Ln-UCs, the QDs transfer emissive energy via luminescence radiative energy transfer (LRET) to a lanthanide sensitizer, which subsequently transfers energy to activators. Direct sensitization of Ln-UCs by QDs is an ongoing research challenge. One of the most significant challenges is that the emission bandwidth from QDs is typically spectrally broader than the absorption of the lanthanide. As a result, not all of the light emitted by the QD sensitizer can be absorbed by the lanthanide upconverter. An important advantage of using QDs to sensitize Ln-UCs for bioapplications is their ability to be stable in aqueous environments without sacrificing photostability, which is a major issue with organic dye molecule sensitizers.[10]

In a recent study, Song et al. looked at improving UCL in Nd^{3+}/Yb^{3+}-sensitized Ln-UC systems with the addition of Ag_2Se QD sensitizers. Co-sensitization with Nd^{3+} and Yb^{3+} is a popular approach when developing Ln-UC for biological applications because it

Accepted Manuscript
Version of Record at: https://doi.org/10.1021/acsaom.3c00067

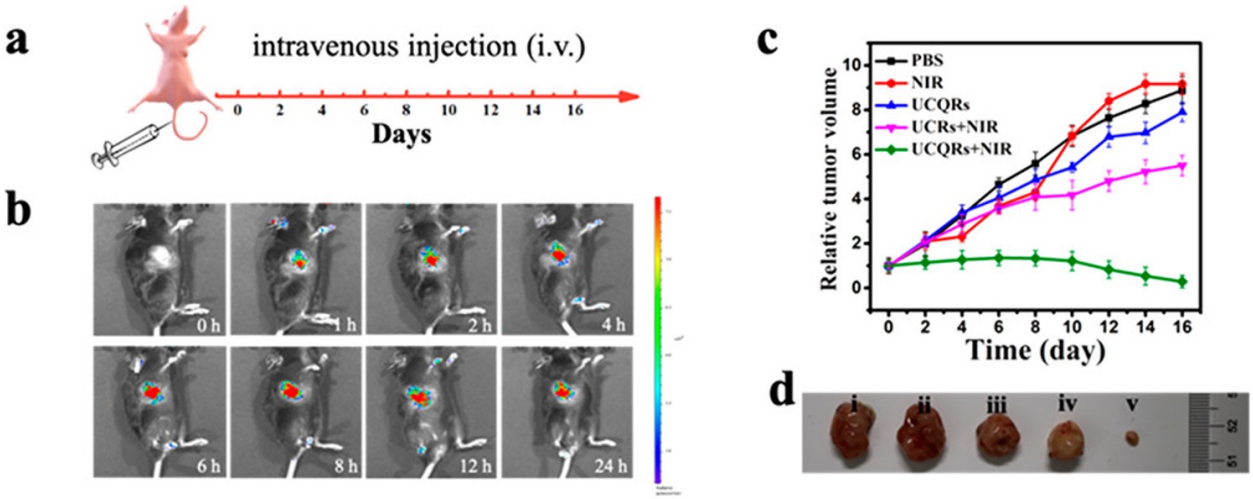

Figure 4: Results of in vivo antitumor treatment by photodymanic therapy using QD-sensitized Ln-UC (UCQR) under NIR illumination to activate the photosensitizer Rose Bengal. (a) Schematic of treatment plan using I.V. tail injection and monitoring for 16 days post-injection. (b) Fluorescence imaging showing location of UCQR at various time points post-injection. (c) Plot of relative tumor volumes and (d) representative photographs of excised tumors from the different treatment groups. Reproduced from ref 7. Copyright 2019 American Chemical Society.

avoids using 980nm excitation. Nd^{3+} absorbs light at 808nm and transfers energy to Yb^{3+}, which can then transfer energy to a variety of Ln^{3+} activators. Unfortunately, using Nd^{3+} as a sensitizer poses new problems. Because the energy level structure of Nd^{3+} is far more complex than that of Yb^{3+} there is an increased likelihood of the Nd^{3+} sensitizers deactivating the emitters rather than activating them. This ultimately hurts the UCL efficiency.[38] In this study, Ag_2Se QDs with absorption and emission energies ranging from 810-870nm and 965-985nm, respectively, were attached to the surface of two types of Yb^{3+}-sensitized Ln-UC nanoparticles by coencapsulation with amphiphilic phosphatidylcholine. When illuminated with 808nm light, UCL was observed at 545nm for $NaYF_4$:Yb^{3+}/Gd^{3+}/Er^{3+} and 480nm for $NaYF_4$:Yb^{3+}/Gd^{3+}/Tm^{3+} particles. They also examined if the addition of Ag_2Se QDs to Nd^{3+}/Yb^{3+} cosensitized Ln-UCs, where Nd^{3+} can directly absorb the 808nm excitation, would improve UCL. In these measurements they found that Ag_2Se drastically improved UCL efficiency in the cosensitized system, likely from improved absorption efficiency of the 808nm light due the large absorption cross section of the QDs compared to Nd^{3+}.

Song et al. also demonstrated the use of these UCNP-QDs nanocomposites to activate a photosensitizer (PS) for photodynamic therapy (PDT) of cancerous tumor cells in mice. PDT is a non-invasive, light-activated method for local treatment of diseases. In general, PDT uses a PS molecule that, when activated in the presence of oxygen, generates reactive oxygen species that are toxic to cells in the local area.[39] As shown in Figure 4, Song et al. split the mouse subjects into five different treatment groups. The first three groups served as controls receiving either only a saline injection, only NIR irradiation, or only injection of UCNP-QDs. As shown in Figure 4c, all three groups showed a similar increase in tumor size over the course of the trial. The two experimental groups received injections of either UCNPs without QDs or the UCNP-QDs nanocomposites and also were irradiated with NIR light. The results showed that while both groups performed better than the control groups, only the group that received the UCNP-QDs injection had a net decrease in tumor size over the duration of the trial. Other measurements confirmed that the UCNP-QDs were biocompatible and could be delivered to the tumor effectively by either direct intratumor injection or intravenous tail injection.

QD-sensitized Ln-UCs have been used for other bioapplications as well. In 2020, Yu et al. took advantage of the distance-dependent nature of the LRET process in these systems to develop a biosensor to target thrombin.[10] They again used Ag_2Se QDs with strong emission at 980nm to sensitize $NaYF_4$:Yb^{3+}/Er^{3+} nanocrystals. The surfaces of both the QDs and Ln-UC were modified with thrombin aptamers, as shown in Scheme 1 of Figure 5. Thus, when thrombin was introduced to the system, the QDs and Ln-UCs were brought into close proximity of each other through the formation of a thrombin-aptamer complex, leading to effective energy transfer between the two species. The amount of thrombin in the system could be quantified by measuring the increase in UCL due to the energy transfer from the QDs. They found that the biosensor had a very high signal-to-background ratio and good sensitivity towards the target when tested on real human plasma samples.

While lanthanide UCs sensitized with QDs are of particular interest for bioapplications

Accepted Manuscript
Version of Record at: https://doi.org/10.1021/acsaom.3c00067

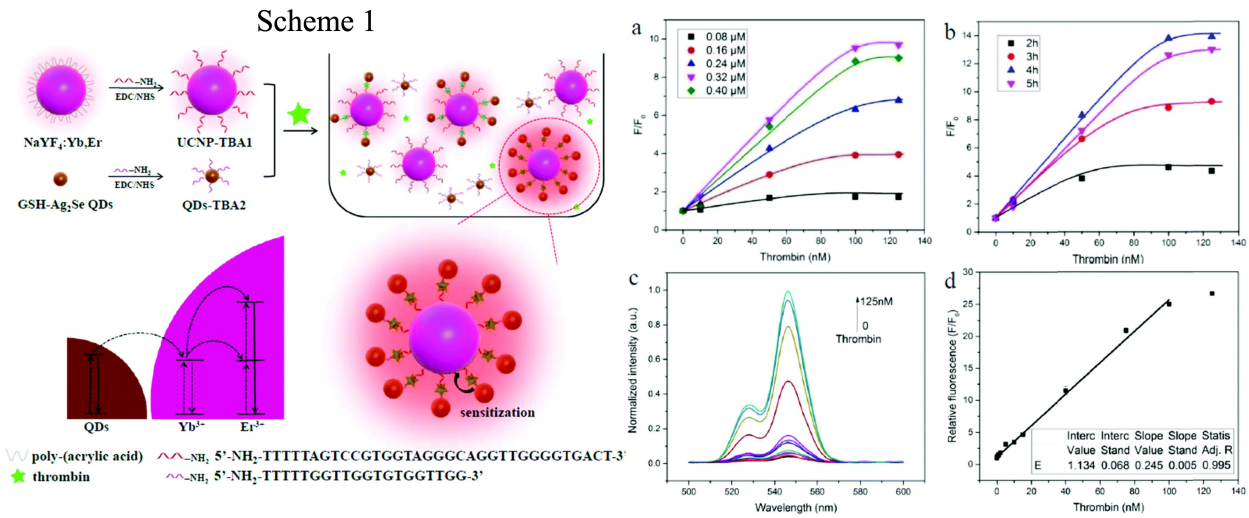

Figure 5: Scheme 1 demonstrates the working principle of a thrombin biosensor using Ag_2Se QD-sensitization enhancement of $NaYF_4$:Yb^{3+}/Er^{3+}. UCL enhancement as a function of thrombin concentration varying with (a) QD-TBA2 concentration and (b) reaction time. (c) UCL spectra of biosensor with increasing thrombin concentration. (d) Linear relationship between UCL enhancement and thrombin concentration. Reproduced with permission from ref 10. Copyright 2020 The Royal Society of Chemistry.

for the reasons explained above, these systems can also be used for solar energy harvesting. In 2010, Pan et al. reported on using PbS QDs coupled to a commercially available Yb^{3+}/Er^{3+} Ln-UC to improve the efficiency of a bifacial silicon solar cell.[40] They measured up to 60% larger increase in photocurrent when the QDs were incorportated compared to using only the Ln-UCs. Unfortunately, they were not able to determine if the PbS QDs were serving as a sensitizer for the lanthanide ions, or if scattering from the QDs simply increased absorption within the Er^{3+} ions. Additionaly, the researchers noted that Yb^{3+}/Er^{3+} upconverters are not ideally suited to combine with silicon solar cells due to the Yb^{3+}/ absorption at 980 nm being higher in energy than the silicon bandgap (1100 nm).

4. Upconversion in TTA-Semiconductor Systems

TTA is a process that occurs in certain organic molecular systems consisting of a sensitizer species and an emitter (or acceptor) species. A sample upconversion mechanism in a TTA

Accepted Manuscript
Version of Record at: https://doi.org/10.1021/acsaom.3c00067

system is depicted schematically in Figure 6. First, a sensitizer molecule is excited from the ground singlet state (S_0) to the excited singlet state (S_1) by absorption of a low-energy photon ($h\nu_1$). The molecule then relaxes to the excited triplet state (T_1) by intersystem crossing (ISC). Energy is then transferred from the sensitizer molecule to an emitter molecule via triplet-triplet energy transfer (TTET), generating an emitter in the excited triplet state. This process repeats many times to generate a large population of emitters in the triplet excited state. In the final step, two triplet emitters collide and undergo triplet-triplet annihilation (TTA), resulting in one emitter being excited to the S_1 state and the other relaxing to the ground state. The emitter in the S_1 state radiatively relaxes back to the ground state by emitting a high-energy photon ($h\nu_2$).

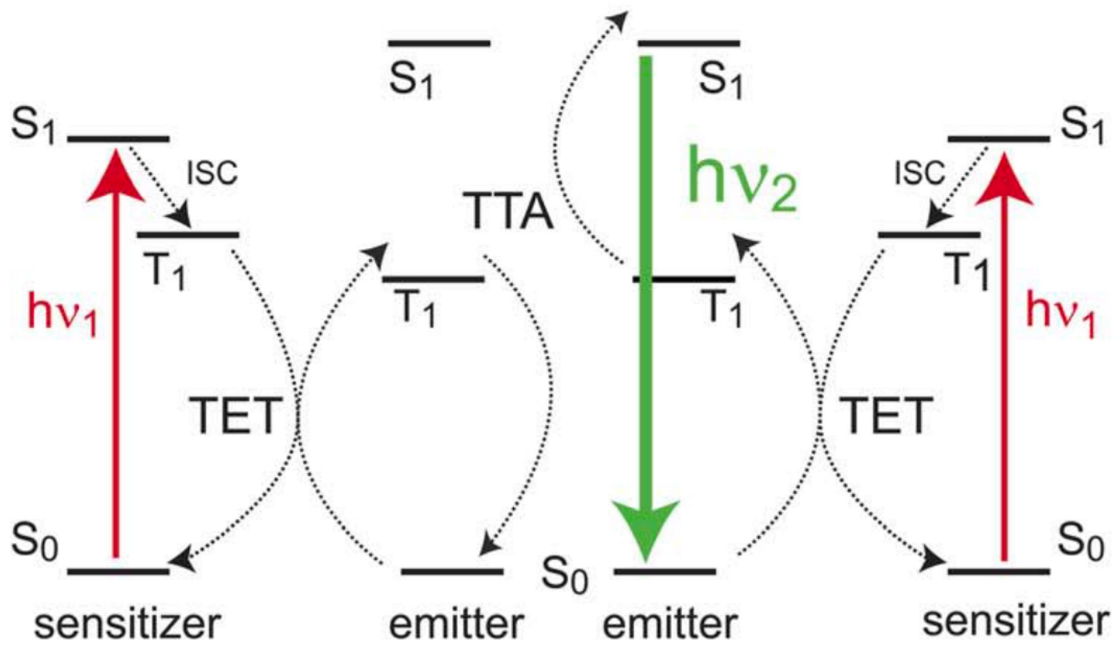

Figure 6: Representative upconversion mechanism for a TTA system. Sensitizer molecules are excited to a triplet state by absorption of low-energy photons followed by intersystem crossing. The energy is transferred to emitter molecules by triplet energy transfer and triplet-triplet annihilation between two emitters generates one emitter excited to a high energy singlet state. Radiate recombination of the excited emitter results in upconversion luminescence. Reproduced with permission from ref 41. Copyright 2012 The Royal Society of Chemistry.

TTAs have a few advantages over Ln-UC systems. First, the organic molecules used in TTAs have much stronger absorption than lanthanide ions, resulting in a lower excitation power density threshold (>1mW cm^{-2} for TTA compared to >1W cm^{-2} for Ln-UC).[27] Additionally, TTAs have recorded the highest efficiencies, with some systems demonstrating over 30% efficiency.[42] However, TTAs also have several drawbacks. The highest UCQYs in TTAs have been measured in solution, but for many applications a solid state upconverter is required. TTA upconversion in solid polymer matrices has been demonstrated, but UCQY is significantly reduced due to reduced mobility of the sensitizer and annihilator species, which must come in close proximity of each other for the energy transfer process to occur.[16] Additionally, the multiple relaxation steps in the TTA process introduces a large PES in these systems that can limit the upconversion energy gain. Finally, while TTAs are often seen as a more tunable platform than Ln-UCs due to the large number of organic sensitizer-emitter pairs available, it has proven difficult to find organic sensitizers that absorb strongly at wavelengths longer than 750nm, thus limiting their use in NIR-absorbing upconversion applications. The organic sensitizers that do absorb in this region also tend to have lower photostability and undergo rapid internal conversion to the ground state.[43,44] For this reason, coupling TTA upconverters to inorganic sensitizers that absorb in the red and NIR regions is a promising route to expand the spectral range of TTAs. In recent years, there have been many demonstrations of TTAs sensitized with a range of inorganic materials including TMDs,[45] bulk[46,47] and nanocrystalline[48–50] perovskites, and semiconductor quantum dots.[15,43,51–53] For the purposes of this review, we will focus exclusively on examples using nanocrystalline materials.

There have been several demonstrations of successful sensitization of TTAs with II-VI and IV-VI QDs for both NIR-to-visible and visible-to-UV upconversion.[15,43,51–53] For example, Mahboub et al. used PbS/CdS core/shell QDs to develop a hybrid TTA platform. The QDs served as a sensitizer with 5-carboxylic tetracene (5-CT) as a transmitter and rubrene as the annihilator. The energy transfer mechanism is shown in Figure 7a. Upon excitation at

808nm, UCL at 560nm, corresponding to the emission spectrum of rubrene (Figure 7b), was measured with a maximum UCQY of 8.4%.

Most of the work on QD sensitizers for TTA UC has focused on two types of QD surface modifications as a way to improve the UCL efficiency. The first modification is the addition and optimization of a passivating shell. Growing a shell of wider-bandgap material onto a core QD is a commonly used practice to improve the PLQY and stability of the core QD.[54] In the study by Mahboub, addition of a thin CdS shell to the PbS core QDs reasulted in an increase in UCQY. However, beyond a certain shell thickness UCQY begins to decrease again, as demonstrated in Figure 7c. This behavior is attributed to the increase in distance between the PbS QD and the transmitter 5-CT molecules, resulting in a reduction in their wave function overlap and less efficient energy transfer. Therefore, there is an ideal shell thickness at which the PLQY of the core QDs is optimized before the rapid decrease in energy transfer efficiency begins to dominate. A similar trend has been observed in other systems.[15,52,53] Another important parameter in optimizing the core/shell structure of QD sensitizers is selecting an appropriate shell material. Huang et al. demonstrated this in a 2018 study of CdSe QD sensitizers for a TTA system using 9-anthracenecarboxylic acid (9-ACA) transmitter and diphenylanthracene (DPA) annihilator. The CdSe QDs were coated with both CdS and ZnS shells of varying thicknesses. While addition of the ZnS shell produced results similar to previous studies (increasing then decreasing UCQY with increasing shell thickness), addition of the CdS shell resulted in poor UCQY regardless of shell thickness.[52] This result is suprising as CdS is widely used to passivate CdSe QDs and can result in incredibly high PLQYs.[55,56] In this case, while the CdS shell did increase the PLQY of the CdSe shell, it also increased the exciton-phonon coupling because the exciton is delocalized within the shell due to minimal conduction band offset between CdSe and CdS. This significantly reduces the efficiency of the energy transfer process, thus hurting the UCQY. These studies on shell thickness and composition show that the design parameters typically used for optimizing PLQY in QDs cannot necessarily be directly applied when working with QD-TTA systems.

Accepted Manuscript
Version of Record at: https://doi.org/10.1021/acsaom.3c00067

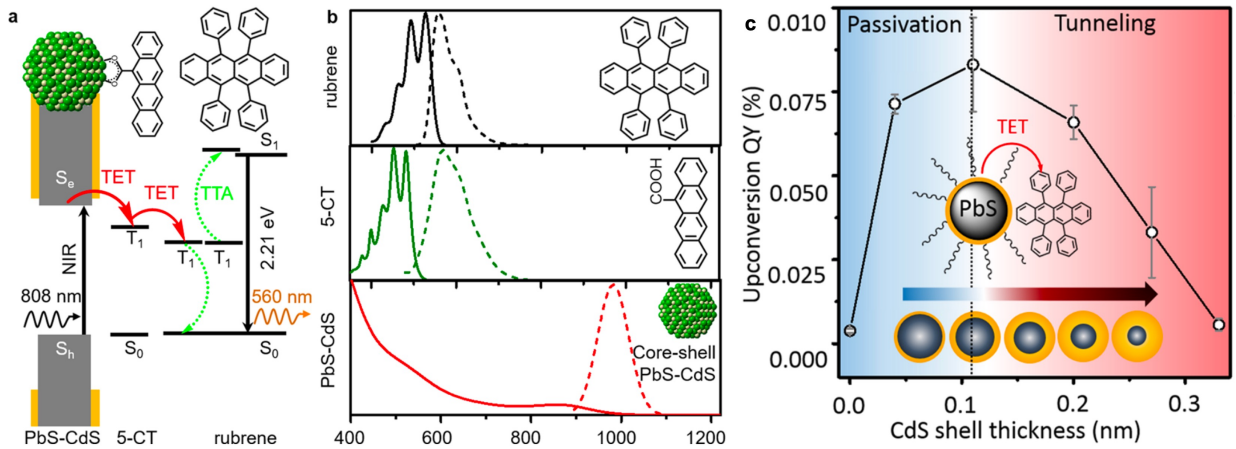

Figure 7: (a) Diagram of upconverison mechanism in QD-TTA system. PbS/CdS QDs (sensitizer) absorb low energy photons and transfer energy to surface-bound 5-CT ligands (transmitter), which mediate TTET to rubrene (annihilator). Rubrene then undergoes TTA to generate upconverted light. (b) Absorption (solid) and emission (dashed) spectra of rubrene (top), 5-CT (middle), and PbS/CdS QDs (bottom). (c) UCQY as a function of increasing CdS shell thickness. Reproduced from ref 43. Copyright 2016 American Chemical Society.

A second possible surface modification technique to improve UCL is direct functionalization of the QD surface with the transmitter molecules. QD surfaces are coated with organic ligands to stabilize and prevent agglomeration of the particles. Ligands are typically determined by the synthesis conditions for the particles, but ligand exchange procedures are commonly used to replace the native ligands to achieve a desired functionality. In the case of QD sensitizers for TTA UC, directly attaching the transmitter ligands to the QD surface can increase the energy transfer efficiency between the two. For example, binding the 5-CT transmitter directly to the PbS/CdS QDs in the example discussed previously led to a 37-fold increase in UCQY, giving rise to the optimized value of 8.4%. Interestingly, the same result was not observed in an analogous visible-to-UV system.[15]

There have also been several demonstrations of QD-sensitized TTA upconversion in solid state devices.[44,46] For example, Wu et al. designed a thin film device consisting of a PbS QD sensitizer layer and an organic rubrene/dibenzotetraphenylperiflanthene (DBP) annihilator/emitter layer. PbS QDs absorb light in the NIR and transfer energy to the lowest triplet

Accepted Manuscript
Version of Record at: https://doi.org/10.1021/acsaom.3c00067

excited state of rubrene. Two rubrene triplets undergo TTA to generate a single rubrene in a singlet excited state, which subsequently transfers energy to the singlet excited state of a DBP emitter. The energy transfer process and a device diagram are shown schematically in Figure 8. The authors demonstrated that this system produced upconversion emission at 612 nm from DBP when excited across a broad range of NIR wavelengths from 800 nm to beyond 1μm. As mentioned previously, TTA systems require the sensitizer and annihilator species to be in close proximity for efficient energy transfer to occur. Wu et al. noted that the highest upconversion efficiencies for their devices were measured where the PbS QD layer was thin, and proposed this was due to both shortened diffusion path lengths and minimized reabsorption. Their best performing device recorded an UC PLQY of 0.57% (74 mw cm^{-}2 808 nm excitation). When normalized to the PLQY of the organic emitting later (46.3%), they determined the upconversion efficiency to be 1.2%.

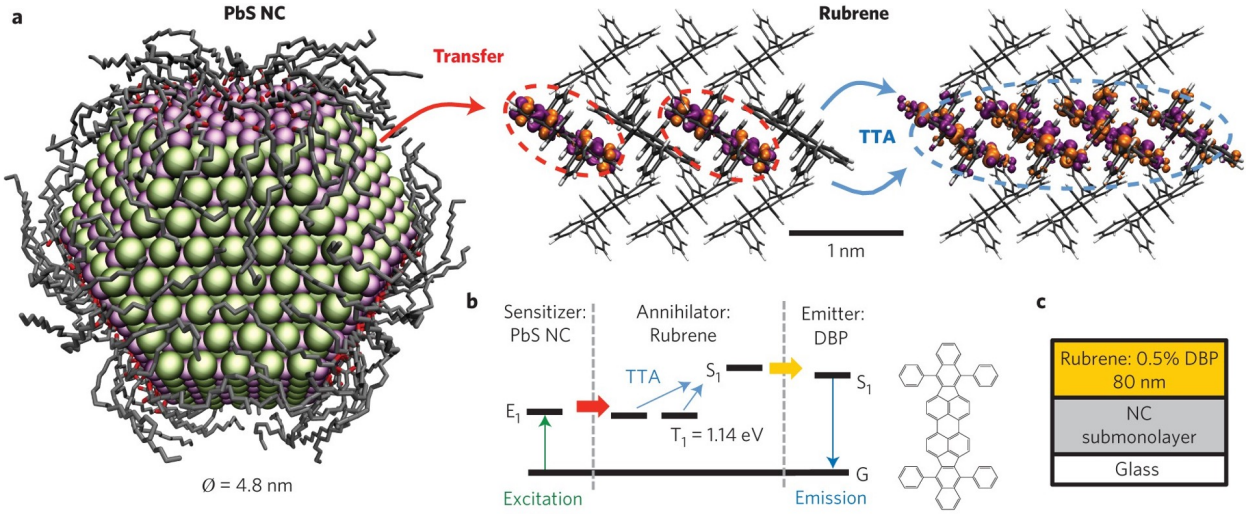

Figure 8: (a) Schematic representations of PbS NC (sensitizer) and Rubrene (triple annihilator). (b) Energy transfer diagram showing the upconversion mechanism in PbS-sensitized rubrene/DBP TTA system. (c) Thin film QD-TTA upconverting device structure. Reproduced with permission from ref 44. Copyright 2015 The Royal Society of Chemistry.

Sensitization of TTAs with perovskite nanocrystals has also been recently been demonstrated.[48–50] In 2017, Mase et al. reported the first use of perovskite sensitized TTA UC using $CdPbX_3$ (X= Br/I) nanocrystals to sensitize DPA resulting in green-to-blue upcon-

Accepted Manuscript
Version of Record at: https://doi.org/10.1021/acsaom.3c00067

version with 1.3% efficiency.[48] More recently, visible-to-UV upconversion has been shown using PeQD sensitizers.[49,50] These materials are particularly interesting for improving the efficiency of photocatalytic processes by, for example, harvesting below bandgap photons for utilization in water splitting catalyzed by wide bandgap semiconductors.[57] He et al. synthesized strongly confined $CsPbBr_3$ PeQDs coated with 1-naphthalene carboxylic acid (NCA) as the triplet transmitter to sensitize UC in 2,5-diphenyloxazole (PPO).[49] They measured an optimized UCQY of 10.2% for this system, a significant improvement over other visible-to-UV TTA upconverters.[15] The high UCQY was attributed to fast and efficient energy transfer due to strong quantum confinement increasing the wavefunction overlap between the PeQDs and NCA triplet acceptors.

5. Upconversion in Semiconductor Nanostructures

The two classes of materials discussed in the prior sections have gained popularity as upconverters because they naturally occur with the necessary electronic state structure for efficient upconversion. Specifically, they have long-lived intermediate states that support either ESA or ETU. Unfortunately, the limitations of these materials also stems from their electronic structure, which is fixed and cannot be tuned to better match the criteria for a desired upconversion application. An alternative approach would be to engineer a material with the desired electronic structure for a particular upconversion application. This idea has given rise to the recent development of upconversion platforms based entirely on complex semiconductor nanostructures.

Unlike Ln-UCs and TTAs, which only allow specific energy transitions between discrete atomic or molecular energy levels, semiconductor UCs have electronic bands with a high density of states, allowing a wide range of transition energies. In general, most SC UCs utilize an ESA mechanism in which the first photon absorption event excites an electron-hole pair via interband absorption and the second photon absorption event further excites

one of those carriers via intraband absorption. The exact ESA mechanism is dependent upon the band structure of the upconverting nanostructure. SC nanostructures are also known to undergo Auger upconversion, which may occur alongside other mechanisms. In fact, Makarov et al. showed it is possible to tailor the electronic structure of the SC nanostructure to either promote or suppress Auger UC.[58]

There have been several reports of photon upconversion via ESA in colloidal QDs.[59–66] These nanostructures typically use Cd/Zn- or Pb-chalcogenide (O, S, Se, Te) semiconductors, termed II-VI and IV-VI, respectively, due to their component elements' locations in the periodic table. Recent advances in the field of colloidal QD synthesis have enabled growth of complex nanoheterostructures comprised of multiple II-VI or IV-VI materials. In 2013, Deutsch et al. demonstrated photon upconversion by ESA in a colloidal double quantum dot system. The heterostructure used consisted of a tellurium-doped CdSe QD [CdSe(Te)] and a CdSe QD spatially separated by a CdS nanorod. As depicted in Figure 9a, upconversion in this system occurs by absorption of two low-energy photons in the CdSe(Te) QD and emission of a higher-energy photon from the CdSe QD. Absorption of the first low-energy photon creates an electron-hole pair localized in the CdSe(Te) QD. However, due to minimal conduction band offset between the materials in the nanostructure, the electron becomes delocalized across the entire structure while the hole remains localized in the CdSe(Te) QD. A second low-energy photon promotes the confined hole to a higher energy valance band state via intraband absorption. This hot-hole is then able to cross the energy barrier between the CdSe(Te) QD and the CdS nanorod and become delocalized across the entire structure. Upconversion emission occurs when both the electron and hole localize in the CdSe QD and radiatively recombine. Following pulsed excitation at 680nm, emission at 570nm is observed, resulting in an energy gain of around 0.35eV.[59]

Deutsch et al. acknowledged that an Auger mechanism could also be responsible for the measured UCL, and designed a two-color excitation experiment to show that ESA was the dominant UC mechanism. Samples were excited with both 680nm and 1064nm laser pulses.

Accepted Manuscript
Version of Record at: https://doi.org/10.1021/acsaom.3c00067

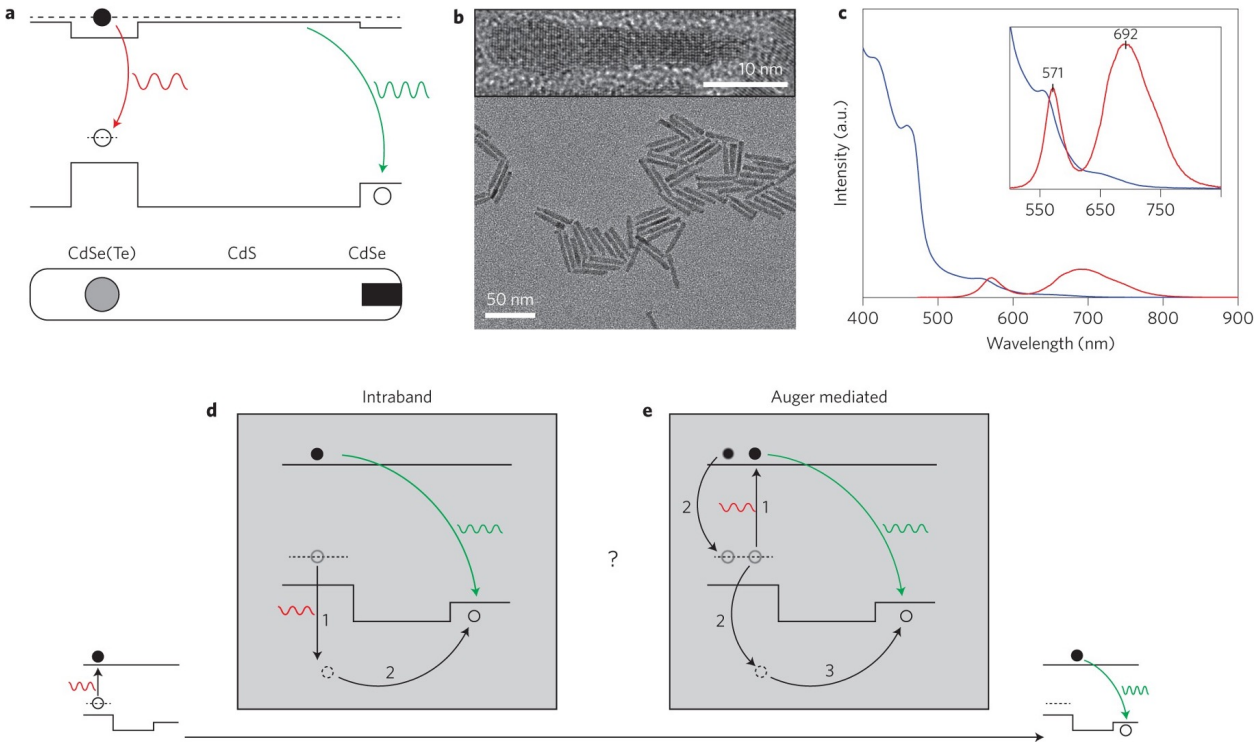

Figure 9: (a) Schematic band diagram of CdSe(Te)/CdS/CdSe dot-rod-dot upconverter. (b) HR-TEM image of nanocrystals. (c) Absorbance (blue) and PL (red) spectra showing dual emission peaks from nanostructure. (d and e) Diagrams of two potential upconversion mechanisms - Intraband Absorption (ESA) or Auger upconversion. Reproduced with permission from ref 59. Copyright 2013 Springer Nature.

While 680nm excitation is high enough in energy to drive both the interband and intraband photon absorptions, 1064nm only provides enough energy for the intraband absorption. Upon addition of the 1064nm excitation they saw an increase in the UCL, indicating that ESA was occuring in this system. If Auger UC was the only mechanism, the UCL signal would be unchanged by addition of the 1064nm light because the Auger process relies only on interband photon absorption. While the UCQY of this system was not measured directly, the UC efficiency upon hot-hole generation was estimated to have a maximum value of 0.1%. This value is limited by both the probability of the hot-hole crossing the energy barrier and the radiative quantum yield of the 570nm emission. This work demonstrated the feasibility of creating a tunable upconversion platform from colloidal semiconductor QDs, but the system required signficant optimization in order to compete with existing higher efficiency UC materials.

In 2019, Milleville et al. built on the work by Deutsch and showed that it is possible to significantly improve the upconversion efficiency of these colloidal structures by using careful heterostructure engineering. Starting with the same CdSe(Te)/CdS/CdSe dot-rod-dot structure, they made two key changes to the design of the nanostructure. The first was improving the alloying in the CdSe(Te) QD to remove potential trap states. Due to the difference in reactivity between Se and Te, CdSe(Te) QDs have been shown to form inhomogeneous alloys with a Te-rich center and a Se-rich shell, creating potential surface trap states as shown in Figure 10b (Sample A).[67] By modifying the concentration ratios of the Cd-, Se-, and Te- precursors during synthesis, they were able to create a homogeneous alloyed CdSe(Te) QD and improve the UCQY by a factor of two. The second modification to the structure was in the CdS nanorod. Originally, the nanorod served simply to allow for delocalization of an excited electron across the entire structure. However, given the essentially flat conduction band potential, the electron was likely to stay in the CdSe(Te) QD rather than migrate to the CdSe QD. A unique feature of semiconductor nanostructures is that the electronic potential can be tailored by changing the size or composition of the

Accepted Manuscript
Version of Record at: https://doi.org/10.1021/acsaom.3c00067

structure. In this case, a gradient potential was formed in the CdS nanorod by adding increasing amounts of the narrower-bandgap material CdSe. This created a tapered bandgap to "funnel" carriers towards the CdSe QD (Figure 10b, Sample B). By combining these two structural modifications, an optimized upconverting nanostructure (Sample D) was realized.

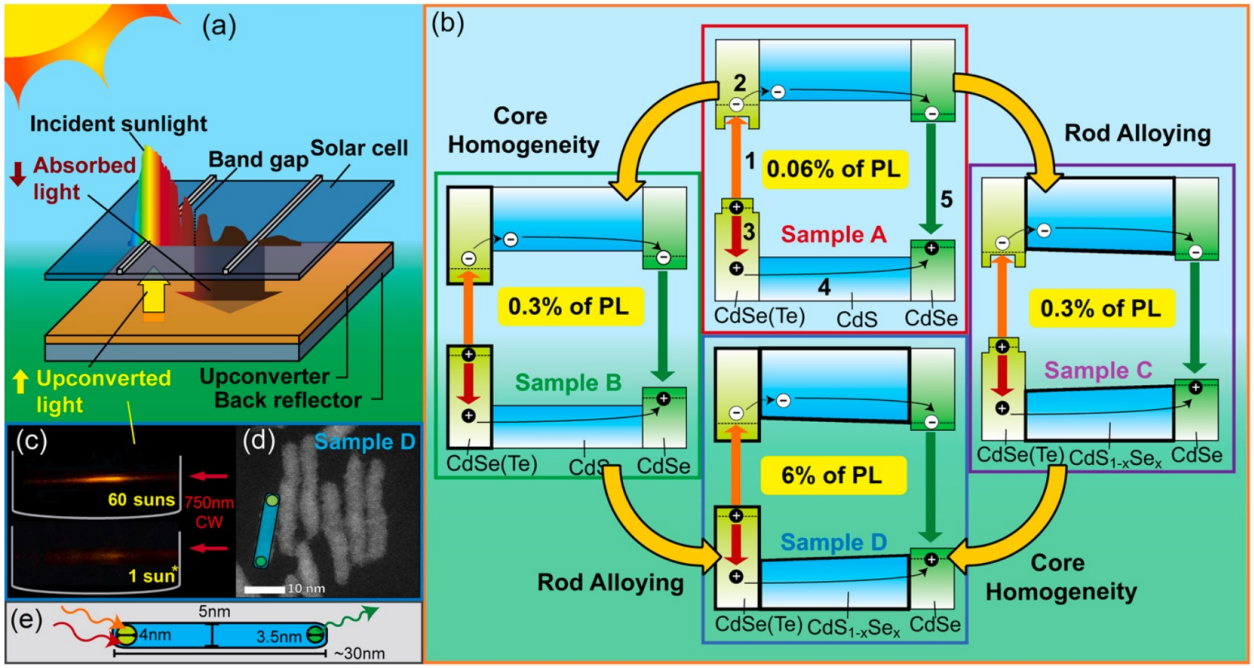

Figure 10: (a) Schematic representation of an upconverter-backed solar cell. (b) Band structures and UCE of four variations of dot-rod-dot UC nanostructures optimized using heterostructure engineering. (c) Photographs of UCL from sample D under 750nm CW illumination with power density equivalent to 60 suns (top) and 1 sun (bottom). (d) TEM image of dot-rod-dot nanostructure. (e) Schematic showing absorption of low energy photons and emission of high energy photons from different regions of the heterostructure. Reproduced from ref 63. Copyright 2019 American Chemical Society.

In Milleville study, the UCQY of all four samples was directly measured and ranged from 2×10^{-4} (Sample A) to 2×10^{-3} (Sample D), suggesting an order of magnitude improvement in UCQY due to the heterostructure engineering. However, when the UCQY measurements were normalized by the CdSe PLQY (i.e. accounting for differences in the PLQY of the CdSe emitters in each family of upconversion heterostructures), the optimized structure (Sample D in Figure 10b.) showed a 100-fold increase in performance over the original dot-rod-dot structure. Importantly, all UCL measurements in the Milleville study were conducted

Accepted Manuscript
Version of Record at: https://doi.org/10.1021/acsaom.3c00067

using CW excitation and UCL was observed under solar-relevant excitation fluxes. This was an important demonstration because the wide AB of SC nanostructures makes them particularly suited for solar energy harvesting upconversion applications. While the UCQY values reported by Milleville, et al. are still incredibly low when compared to Ln-UCs and TTAs, this work showed that there is significant potential for continued improvement as we gain better understanding and control over the effects of nanoparticle structure on the upconversion process.

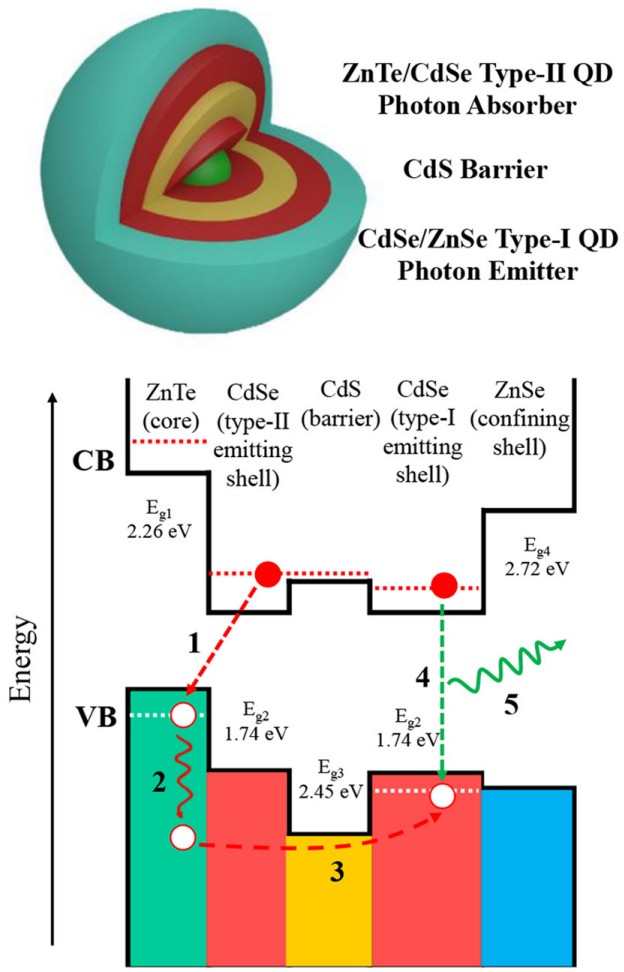

Figure 11: Schematic illustration (top) and band diagram (bottom) of ZnTe/CdSe@CdS@CdSe/ZnSe core/multi-shell upconverting QD structure. A Low energy photon is absorbed in the ZnTe/CdSe core via an indirect interband transition, leaving a confined hole and a delocalized electron. The second low energy photon promotes the confined hole over the energy barrier via intraband absorption. Readiative recombination of the electron and hole in the CdSe outer shell results in UCL. Reproduced from ref 66. Copyright 2021 American Chemical Society.

The previous two examples used an elongated nanorod structure to realize photon upconversion. Upconversion has also been demonstrated in core/multi-shell particles.[61,64,66] For example, Yang et al. designed a 5-layer structure that emits at 635nm under 820nm excitation. The structure, shown in Figure 11, consists of a ZnTe/CdSe absorber core, a CdS barrier layer, a CdSe emitting shell, and a ZnSe confining shell.[66] There are two important feature of this design that make it ideal for photon upconversion. First is the use of a ZnTe/CdSe core/shell heterostructure as the low-energy photon absorber. These materials exhibit a Type-II band alignment, meaning the first low-energy photon is absorbed via an indirect interband transition that generates an electron localized in the CdSe region and a hole localized in the ZnTe region. The UC mechanism then proceeds much in the same way as for the systems already discussed above, with the electron delocalized across the structure while the hole is further excited via an intraband absorption to cross the energy barrier. The spatial separation of the electron and hole in this Type-II structure leads to longer exciton lifetimes, increasing the time window in which upconversion can occur and decreasing the necessary photon flux. The Type-II absorber also has a narrower energy gap, which means that longer wavelength excitation sources can be used, resulting in a larger upconversion energy gain. Second, the use of a ZnSe confining outer layer serves to improve the emission efficiency from the CdSe layer. Poor emission quantum yield in the high energy emitter significantly limits the UCQY in all SC UC structures. Yang showed that upon addition of the ZnSe shell, the PLQY of the CdSe emitter increased from 5% to 46%. In this case the ZnSe shell passivates the surface of the CdSe in the same way as for the TTA-QD systems discussed previously. In the pure semiconductor system, however, the exact thickness of this shell is not a crucial design factor because there is no distance-dependent energy transfer process occurring. Finally, Yang acknowledged that most studies of UC in semiconductor QDs are carried out in solution, which is not practical for many proposed applications. As a proof-of-concept experiment, Yang prepared an upconverting QD film via spin-coating. While the luminescent properties of the QDs were diminished in the film, UCL was still

observed.

While the majority of reports of upconversion in semiconductors have used colloidal II-VI and IV-VI heterostructures, there are other possible semiconductor upconversion material platforms. Of particular interested are III-V semiconductors, which can be grown in complex heterostructures with exceptional optical properties via techniques such as molecular beam epitaxy. There have been several reports of upconversion in III-V materials, but many rely on SHG or TPA mechanisms and thus require very high excitation fluxes.[68–71] Recently there have been some reports of III-V upconverters using an ESA mechanism, but efficiencies remain low, particularly at low excitation powers.[72,73] Recently Jansson et al. reported on upconversion in GaAs/GaNAs and GaAsP/GaNAsP core/shell nanowires (NWs) with a focus on improving low-power upconversion efficiency.[74] The upconversion mechanism in these structures is shown in Figure 12c. First, a low-energy photon is absorbed to generate an electron and hole in the narrower-bandgap shell. Next, the electron is further excited by absorption of a second photon and transfers into the larger-bandgap core. Finally, UCL results from radiative recombination of the electron and hole in the core of the NW. This mechanism is heavily dependent on the lifetime of the initial exciton because there is no mechanism to suppress radiative recombination of the carriers in the shell.

Upconversion luminescence in the system developed by Jansson was successfully measured under CW excitation with excitation power densities as low as 0.1 W/cm^2. UCQY was not measured directly in this work, but an upconversion efficiency was calculated based on the relative intensities of PL and UCPL in these structures. Those measurements gave an UCE on the order of 1%, which was similar to other semiconductor nanostructures for which a comparable value could be determined. To further improve UCE, they took advantage of a known property in these NW structures: the dielectric environment, for example a substrate material, can have significant impact on the electric field distribution within the NW. Finite difference time domain simulations suggested that placing the NWs on a gold substrate would help to confine excitation photons within the NW shell and improve UCE.

Accepted Manuscript
Version of Record at: https://doi.org/10.1021/acsaom.3c00067

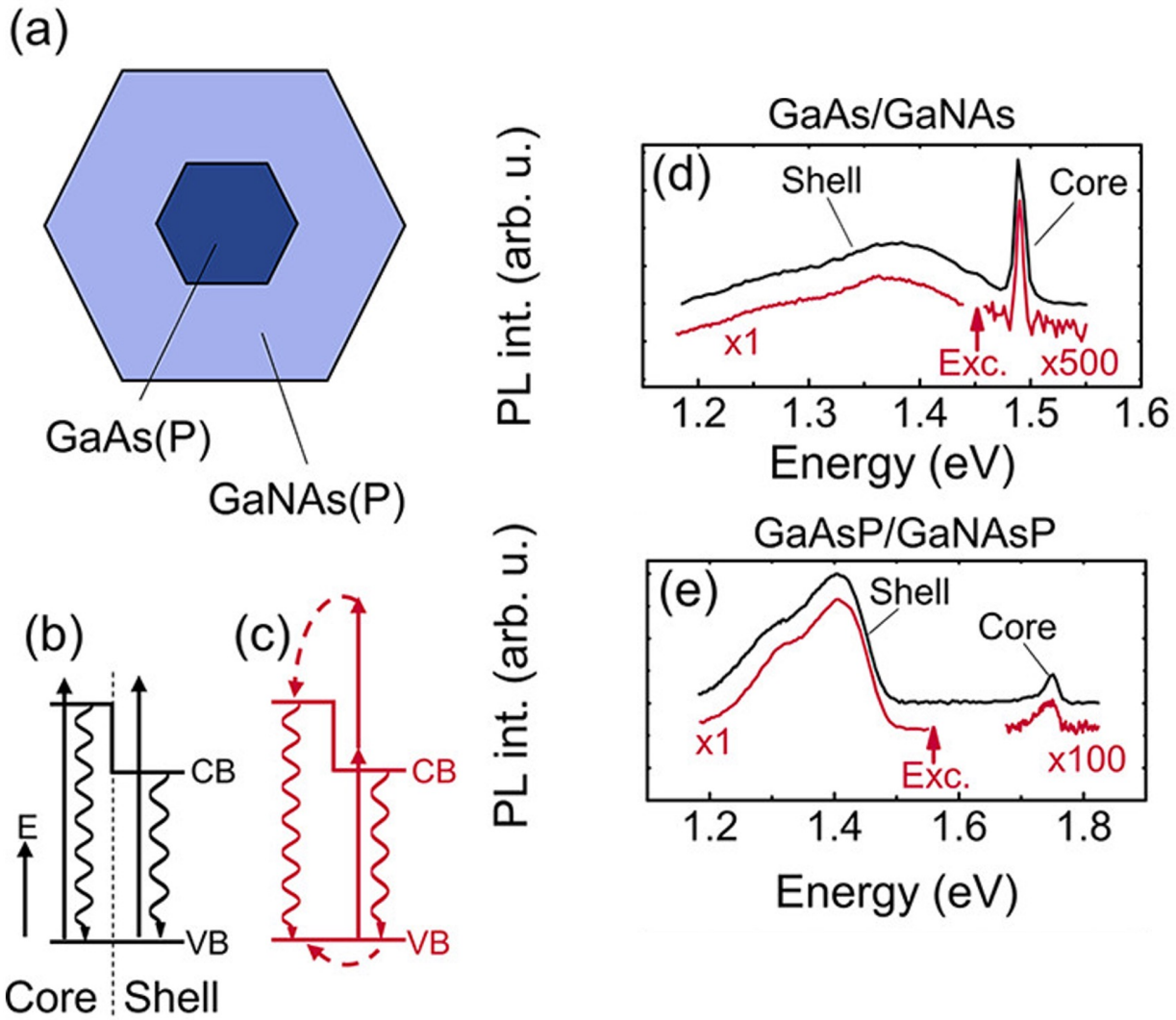

Figure 12: (a) Cross-sectional schematic of III-V core/shell nanowires. (b and c) Energy structure and carrier generation mechanism for excitation energies above (b) and below (c) the core bandgap. (d and e) Emission spectra for GaAs/GaNAs (d) and GaAsP/GaNAsP (e) core/shell NWs for both traditional PL (black) and upconversion PL (red). Reproduced from ref 74. Copyright 2022 American Chemical Society.

Accepted Manuscript
Version of Record at: https://doi.org/10.1021/acsaom.3c00067

Experimental measurements confirmed this effect, resulting in a maximized UCE of 6.7% for GaAsP/GaNAsP core/shell NWs on gold.

6. Conclusions

This review has summarized the role semiconductor nanostructures can play in a range of photon upconversion platforms. Lanthanide-based upconverters have been studied and optimized for several decades, resulting in relatively efficient upconversion materials with demonstrated applications in several fields. However, Ln-UCs still suffer from small absorption bandwidth, limited spectral tunability, and low UCQY that limit their usefulness for certain applications. Similarly, TTA systems have demonstrated record upconversion efficiencies, but lack the broad absorption - particularly in the NIR - needed for solar energy harvesting upconversion applications. Researchers have successfully showed that these systems can be coupled to semiconductor QDs to take advantage of the excellent SC absorption and emission properties. Coupling Ln-UCs or TTAs to QDs as a sensitizer or emitter typically decreases the upconversion efficiency due to the additional energy transfer step. However, the improved spectral utilization afforded by the QDs may make these systems ideal for certain applications despite the trade off in efficiency. Future research could focus on expanding the range of semiconductor materials used for sensitization of Ln-UCs. Surface modification of semiconductor materials to improve energy transfer efficiency is also a potential pathway to improving the performance of semiconductor nanoparticles as both sensitizers and emitters for lanthanide or TTA upconversion systems.

A more recent development has been to design upconversion platforms entirely out of semiconductor nanostructures by taking advantage of the size-, shape-, and composition-dependent nature of the electronic structure in these materials. In roughly one decade of work, upconversion has been demonstrated in a range of SC nanostructures utilizing different component materials, particle morphologies, and growth techniques. These systems have

already demonstrated excellent spectral utilization and low excitation power density thresholds, as expected due to the large absorption cross section and distribution of electronic states in SC nanostructures. The major limiting factor for SC upconverters is the low reported UCQY, and more work is required to better understand how changes to particle structure can improve the upconversion efficiency. This is not a trivial task. The mechanisms for the synthesis of even simple core-shell colloidal nanoparticles are not fully understood to the level required for rational predictive synthesis of target structures.[75] SC upconversion structures such as the dot-rod-dot or core/multi-shell structures are significantly more complex. Future research should likely aim to engineer the bandgap, band offsets, and size of semiconductor nanoparticle heterostructures in order to improve upconversion efficiency through better control of carrier transfer and loss. However, careful, systematic, and time-consuming studies are often needed to determine appropriate synthesis conditions for particles with increasingly complex structures and compositions, and such work is a prerequisite for the analysis of the relationship between particle structure and upconversion efficiency.[76–79]

As the number of potential applications for upconversion has increased, it has become apparent that one single upconversion platform will not be able to meet the requirements of all possible applications. The importance of factors such as large absorption bandwidth, high upconversion efficiency, or large upconversion energy gain varies significantly between different applications. The work highlighted here demonstrates the feasibility of integrating a new class of materials with ideal optical properties (i.e. semiconductor nanostructures) into the existing range of upconversion materials to begin building a library of upconversion platforms that will span the broad range of requirements for the growing number of upconversion applications.

Acknowledgement

The authors acknowledge support from the Delaware Energy Institute. T.A.W. and J.M.C. acknowledge support from the Delaware Space Grant College and Fellowship program (NASA Grant 80NSSC20M0045). M.F.D. acknowledges partial support from the NSF through the University of Delaware Materials Research Science and Engineering Center (MRSEC), DMR-2011824, including partial support of this project through the MRSEC-affiliated Partnership for Research and Education (PREM) in Soft Matter Research & Technology and Quantum Confinement Materials Design (SMaRT QD), DMR-2122158.

References

(1) Bloembergen, N. Solid state infrared quantum counters. *Physical Review Letters* **1959**, *2*, 84–85.

(2) Auzel, F. Upconversion and Anti-Stokes Processes with f and d Ions in Solids. *Chemical Reviews* **2004**, *104*, 139–173.

(3) Hao, C.; Wu, X.; Sun, M.; Zhang, H.; Yuan, A.; Xu, L.; Xu, C.; Kuang, H. Chiral Core-Shell Upconversion Nanoparticle@MOF Nanoassemblies for Quantification and Bioimaging of Reactive Oxygen Species in Vivo. *Journal of the American Chemical Society* **2019**, *141*, 19373–19378.

(4) Yang, G.; Yang, D.; Yang, P.; Lv, R.; Li, C.; Zhong, C.; He, F.; Gai, S.; Lin, J. A Single 808 nm Near-Infrared Light-Mediated Multiple Imaging and Photodynamic Therapy Based on Titania Coupled Upconversion Nanoparticles. *Chemistry of Materials* **2015**, *27*, 7957–7968.

(5) Viger, M. L.; Grossman, M.; Fomina, N.; Almutairi, A. Low power upconverted near-IR light for efficient polymeric nanoparticle degradation and cargo release. *Advanced Materials* **2013**, *25*, 3733–3738.

(6) Zhang, D.; Wen, L.; Huang, R.; Wang, H.; Hu, X.; Xing, D. Mitochondrial specific photodynamic therapy by rare-earth nanoparticles mediated near-infrared graphene quantum dots. *Biomaterials* **2018**, *153*, 14–26.

(7) Song, D.; Chi, S.; Li, X.; Wang, C.; Li, Z.; Liu, Z. Upconversion System with Quantum Dots as Sensitizer: Improved Photoluminescence and PDT Efficiency. *ACS Applied Materials and Interfaces* **2019**, *11*, 41100–41108.

(8) Luo, Z.; Zhang, L.; Zeng, R.; Su, L.; Tang, D. Near-Infrared Light-Excited Core-Core-Shell UCNP@Au@CdS Upconversion Nanospheres for Ultrasensitive Photoelectrochemical Enzyme Immunoassay. *Analytical Chemistry* **2018**, *90*, 9568–9575.

(9) Li, Q. F.; Ren, S. Y.; Wang, Y.; Bai, J. L.; Peng, Y.; Ning, B. A.; Lyu, Q. J.; Gao, Z. X. Efficient Detection of Environmental Estrogens Bisphenol A and Estradiol By Sensing System Based on AuNP-AuNP-UCNP Triple Structure. *Chinese Journal of Analytical Chemistry* **2018**, *46*, 486–492.

(10) Yu, T.; Wei, D. M.; Li, Z.; Pan, L. J.; Zhang, Z. L.; Tian, Z. Q.; Liu, Z. Target-modulated sensitization of upconversion luminescence by NIR-emissive quantum dots: A new strategy to construct upconversion biosensors. *Chemical Communications* **2020**, *56*, 1976–1979.

(11) Deng, R.; Qin, F.; Chen, R.; Huang, W.; Hong, M.; Liu, X. Temporal full-colour tuning through non-steady-state upconversion. *Nature Nanotechnology* **2015**, *10*, 237–242.

(12) Kataria, M.; Yadav, K.; Nain, A.; Lin, H. I.; Hu, H. W.; Paul Inbaraj, C. R.; Chang, T. J.; Liao, Y. M.; Cheng, H. Y.; Lin, K. H.; Chang, H. T.; Tseng, F. G.; Wang, W. H.; Chen, Y. F. Self-Sufficient and Highly Efficient Gold Sandwich Upconversion Nanocomposite Lasers for Stretchable and Bio-applications. *ACS Applied Materials and Interfaces* **2020**, *12*, 19840–19854.

(13) Yang, B.; Wang, Y.; Wei, T.; Pan, Y.; Zhou, E.; Yuan, Z.; Han, Y.; Li, M.; Ling, X.; Yin, L.; Xie, X.; Huang, L. Solution-Processable Near-Infrared–Responsive Composite of Perovskite Nanowires and Photon-Upconversion Nanoparticles. *Advanced Functional Materials* **2018**, *28*, 1801782.

(14) Goldschmidt, J. C.; Fischer, S. Upconversion for photovoltaics - a review of materials, devices and concepts for performance enhancement. *Adv. Opt. Mater.* **2015**, *3*, 510–535.

(15) Gray, V.; Xia, P.; Huang, Z.; Moses, E.; Fast, A.; Fishman, D. A.; Vullev, V. I.; Abrahamsson, M.; Moth-Poulsen, K.; Lee Tang, M. CdS/ZnS core-shell nanocrystal photosensitizers for visible to UV upconversion. *Chemical Science* **2017**, *8*, 5488–5496.

(16) De Wild, J.; Meijerink, A.; Rath, J. K.; Van Sark, W. G.; Schropp, R. E. Upconverter solar cells: Materials and applications. **2011**, *4*, 4835–4848.

(17) Sellers, D. G.; Zhang, J.; Chen, E. Y.; Zhong, Y.; Doty, M. F.; Zide, J. M. O. Novel nanostructures for efficient photon upconversion and high-efficiency photovoltaics. *Solar Energy Materials and Solar Cells* **2016**, *155*, 446–453.

(18) Zhou, J.; Liu, Q.; Feng, W.; Sun, Y.; Li, F. Upconversion luminescent materials: Advances and applications. *Chemical Reviews* **2015**, *115*, 395–465.

(19) Alivisatos, A. P. Semiconductor clusters, nanocrystals, and quantum dots. *Science* **1996**, *271*, 933–937.

(20) Murray, C. B.; Kagan, C. R.; Bawendi, M. G. Synthesis and Characterization of Monodisperse Nanocrystals and Close-Packed Nanocrystal Assemblies. *Annual Review of Materials Science* **2000**, *30*, 545–610.

(21) Jasieniak, J.; Smith, L.; Van Embden, J.; Mulvaney, P.; Califano, M. Re-examination of the size-dependent absorption properties of CdSe quantum dots. *Journal of Physical Chemistry C* **2009**, *113*, 19468–19474.

(22) Chen, E. Y.; Milleville, C.; Zide, J. M.; Doty, M. F.; Zhang, J. Upconversion of low-energy photons in semiconductor nanostructures for solar energy harvesting. **2018**, *5*, E16.

(23) Poles, E.; Selmarten, D. C.; Mićić, O. I.; Nozik, A. J. Anti-Stokes photoluminescence in colloidal semiconductor quantum dots. *Applied Physics Letters* **1999**, *75*, 971–973.

(24) Wang, X.; Qu, L.; Zhang, J.; Peng, X.; Xiao, M. Surface-related emission in highly luminescent CdSe quantum dots. *Nano Letters* **2003**, *3*, 1103–1106.

(25) Zhang, J.; Li, D.; Chen, R.; Xiong, Q. Laser cooling of a semiconductor by 40 kelvin. *Nature* **2013**, *493*, 504–508.

(26) Mergenthaler, K.; Iqbal, A.; Wallentin, J.; Lehmann, S.; Borgström, M. T.; Samuelson, L.; Yartsev, A.; Pistol, M. E. Large-energy-shift photon upconversion in degenerately doped InP nanowires by direct excitation into the electron gas. *Nano Res.* **2013**, *6*, 752–757.

(27) Du, Y.; Ai, X.; Li, Z.; Sun, T.; Huang, Y.; Zeng, X.; Chen, X.; Rao, F.; Wang, F. Visible-to-Ultraviolet Light Conversion: Materials and Applications. *Advanced Photonics Research* **2021**, *2*, 2000213.

(28) Cheng, X.; Zhou, J.; Yue, J.; Wei, Y.; Gao, C.; Xie, X.; Huang, L. Recent Development in Sensitizers for Lanthanide-Doped Upconversion Luminescence. **2021**,

(29) Zhang, Y.; Zhu, X.; Zhang, Y. Exploring Heterostructured Upconversion Nanoparticles: From Rational Engineering to Diverse Applications. **2021**, *15*, 3709–3735.

(30) Yan, C.; Dadvand, A.; Rosei, F.; Perepichka, D. F. Near-IR photoresponse in new upconverting CdSe/NaYF4:Yb,Er nanoheterostructures. *Journal of the American Chemical Society* **2010**, *132*, 8868–8869.

(31) Li, Z.; Zhang, Y.; Jiang, S. Multicolor core/shell-structured upconversion fluorescent nanoparticles. *Advanced Materials* **2008**, *20*, 4765–4769.

(32) Shalav, A.; Richards, B. S.; Trupke, T.; Krämer, K. W.; Güdel, H. U. Application of NaYF4: Er3+ up-converting phosphors for enhanced near-infrared silicon solar cell response. *Applied Physics Letters* **2005**, *86*, 013505.

(33) Zheng, W.; Huang, P.; Gong, Z.; Tu, D.; Xu, J.; Zou, Q.; Li, R.; You, W.; Bünzli, J. C. G.; Chen, X. Near-infrared-triggered photon upconversion tuning in all-inorganic cesium lead halide perovskite quantum dots. *Nature Communications* **2018**, *9*, 1–9.

(34) Zeng, M.; Singh, S.; Hens, Z.; Liu, J.; Artizzu, F.; Van Deun, R. Strong upconversion emission in CsPbBr 3 perovskite quantum dots through efficient BaYF 5 :Yb,Ln sensitization. *Journal of Materials Chemistry C* **2019**, *7*, 2014–2021.

(35) Swarnkar, A.; Chulliyil, R.; Ravi, V. K.; Irfanullah, M.; Chowdhury, A.; Nag, A. Colloidal CsPbBr 3 Perovskite Nanocrystals: Luminescence beyond Traditional Quantum Dots. *Angewandte Chemie* **2015**, *127*, 15644–15648.

(36) Kovalenko, M. V.; Protesescu, L.; Bodnarchuk, M. I. Properties and potential optoelectronic applications of lead halide perovskite nanocrystals. **2017**, *358*, 745–750.

(37) Atre, A. C.; Dionne, J. A. Realistic upconverter-enhanced solar cells with non-ideal absorption and recombination efficiencies. *Journal of Applied Physics* **2011**, *110*, 034505.

(38) Shen, J.; Chen, G.; Vu, A. M.; Fan, W.; Bilsel, O. S.; Chang, C. C.; Han, G. Engineering the upconversion nanoparticle excitation wavelength: Cascade sensitization of tri-doped upconversion colloidal nanoparticles at 800 nm. *Advanced Optical Materials* **2013**, *1*, 644–650.

(39) Yang, D.; Ma, P.; Hou, Z.; Cheng, Z.; Li, C.; Lin, J. Current advances in lanthanide ion (Ln3+)-based upconversion nanomaterials for drug delivery. **2015**, *44*, 1416–1448.

(40) Pan, A. C.; Del Cañizo, C.; Cánovas, E.; Santos, N. M.; Leitão, J. P.; Luque, A. Enhancement of up-conversion efficiency by combining rare earth-doped phosphors with PbS quantum dots. *Sol. Energy Mater. Sol. Cells* **2010**, *94*, 1923–1926.

(41) Cheng, Y. Y.; Fückel, B.; MacQueen, R. W.; Khoury, T.; Clady, R. G. C. R.; Schulze, T. F.; Ekins-Daukes, N. J.; Crossley, M. J.; Stannowski, B.; Lips, K.; Schmidt, T. W. Improving the light-harvesting of amorphous silicon solar cells with photochemical upconversion. *Energy and Environmental Science* **2012**, *5*, 6953–6959.

(42) Wang, B.; Sun, B.; Wang, X.; Ye, C.; Ding, P.; Liang, Z.; Chen, Z.; Tao, X.; Wu, L. Efficient triplet sensitizers of palladium(II) tetraphenylporphyrins for upconversion-powered photoelectrochemistry. *Journal of Physical Chemistry C* **2014**, *118*, 1417–1425.

(43) Mahboub, M.; Huang, Z.; Tang, M. L. Efficient Infrared-to-Visible Upconversion with Subsolar Irradiance. *Nano Letters* **2016**, *16*, 7169–7175.

(44) Wu, M.; Congreve, D. N.; Wilson, M. W.; Jean, J.; Geva, N.; Welborn, M.; Van Voorhis, T.; Bulovic, V.; Bawendi, M. G.; Baldo, M. A. Solid-state infrared-to-visible upconversion sensitized by colloidal nanocrystals. *Nat. Photonics* **2016**, *10*, 31–34.

(45) Duan, J.; Liu, Y.; Zhang, Y.; Chen, Z.; Xu, X.; Ye, L.; Wang, Z.; Yang, Y.; Zhang, D.; Zhu, H. Efficient solid-state infrared-to-visible photon upconversion on atomically thin monolayer semiconductors. *Sci. Adv.* **2022**, *8*, 4935.

(46) Nienhaus, L.; Correa-Baena, J. P.; Wieghold, S.; Einzinger, M.; Lin, T. A.; Shulenberger, K. E.; Klein, N. D.; Wu, M.; Bulović, V.; Buonassisi, T.; Baldo, M. A.; Bawendi, M. G. Triplet-sensitization by lead halide perovskite thin films for near-infrared-to-visible upconversion. *ACS Energy Lett.* **2019**, *4*, 888–895.

(47) Wieghold, S.; Bieber, A. S.; VanOrman, Z. A.; Daley, L.; Leger, M.; Correa-Baena, J. P.;

Nienhaus, L. Triplet Sensitization by Lead Halide Perovskite Thin Films for Efficient Solid-State Photon Upconversion at Subsolar Fluxes. *Matter* **2019**, *1*, 705–719.

(48) Mase, K.; Okumura, K.; Yanai, N.; Kimizuka, N. Triplet sensitization by perovskite nanocrystals for photon upconversion. *Chemical Communications* **2017**, *53*, 8261–8264.

(49) He, S.; Luo, X.; Liu, X.; Li, Y.; Wu, K. Visible-to-Ultraviolet Upconversion Efficiency above 10% Sensitized by Quantum-Confined Perovskite Nanocrystals. *Journal of Physical Chemistry Letters* **2019**, *10*, 5036–5040.

(50) Okumura, K.; Yanai, N.; Kimizuka, N. Visible-to-UV photon upconversion sensitized by lead halide perovskite nanocrystals. *Chemistry Letters* **2019**, *48*, 1347–1350.

(51) Huang, Z.; Li, X.; Mahboub, M.; Hanson, K. M.; Nichols, V. M.; Le, H.; Tang, M. L.; Bardeen, C. J. Hybrid Molecule-Nanocrystal Photon Upconversion Across the Visible and Near-Infrared. *Nano Lett.* **2015**, *15*, 5552–5557.

(52) Huang, Z.; Xia, P.; Megerdich, N.; Fishman, D. A.; Vullev, V. I.; Tang, M. L. ZnS Shells Enhance Triplet Energy Transfer from CdSe Nanocrystals for Photon Upconversion. *ACS Photonics* **2018**, *5*, 3089–3096.

(53) Mahboub, M.; Xia, P.; Van Baren, J.; Li, X.; Lui, C. H.; Tang, M. L. Midgap States in PbS Quantum Dots Induced by Cd and Zn Enhance Photon Upconversion. *ACS Energy Letters* **2018**, *3*, 767–772.

(54) Reiss, P.; Protière, M.; Li, L. Core/shell semiconductor nanocrystals. **2009**, *5*, 154–168.

(55) Carbone, L.; Nobile, C.; De Giorgi, M.; Della Sala, F.; Morello, G.; Pompa, P.; Hytch, M.; Snoeck, E.; Fiore, A.; Franchini, I.; Nadasan, M.; Silvestre, A.; Chioco, L.; Kudera, S.; Cingolani, R.; Krahne, R.; Manna, L. Synthesis and micrometer-scale assembly of colloidal CdSe / CdS nanorods prepared by a seeded growth approach. *Nano Letters* **2007**, *7*, 2942–2950.

(56) Bae, W. K.; Padilha, L. A.; Park, Y.-S.; McDaniel, H.; Robel, I.; Pietryga, J. M.; Klimov, V. I. Controlled Alloying of the Core–Shell Interface in CdSe/CdS Quantum Dots for Suppression of Auger Recombination. *ACS Nano* **2013**, *7*, 3411–3419.

(57) Monguzzi, A.; Oertel, A.; Braga, D.; Riedinger, A.; Kim, D. K.; Knüsel, P. N.; Bianchi, A.; Mauri, M.; Simonutti, R.; Norris, D. J.; Meinardi, F. Photocatalytic Water-Splitting Enhancement by Sub-Bandgap Photon Harvesting. *ACS Applied Materials and Interfaces* **2017**, *9*, 40180–40186.

(58) Makarov, N. S.; Lin, Q.; Pietryga, J. M.; Robel, I.; Klimov, V. I. Auger Up-Conversion of Low-Intensity Infrared Light in Engineered Quantum Dots. *ACS Nano* **2016**, *10*, 10829–10841.

(59) Deutsch, Z.; Neeman, L.; Oron, D. Luminescence upconversion in colloidal double quantum dots. *Nature Nanotechnology* **2013**, *8*, 649–653.

(60) Teitelboim, A.; Meir, N.; Kazes, M.; Oron, D. Colloidal Double Quantum Dots. *Accounts of Chemical Research* **2016**, *49*, 902–910.

(61) Teitelboim, A.; Oron, D. Broadband Near-Infrared to Visible Upconversion in Quantum Dot–Quantum Well Heterostructures. *ACS Nano* **2016**, *10*, 446–452.

(62) Meir, N.; Pinkas, I.; Oron, D. NIR-to-visible upconversion in quantum dots: Via a ligand induced charge transfer state. *RSC Advances* **2019**, *9*, 12153–12161.

(63) Milleville, C. C.; Chen, E. Y.; Lennon, K. R.; Cleveland, J. M.; Kumar, A.; Zhang, J.; Bork, J. A.; Tessier, A.; Lebeau, J. M.; Chase, D. B.; Zide, J. M.; Doty, M. F. Engineering Efficient Photon Upconversion in Semiconductor Heterostructures. *ACS Nano* **2019**, *13*, 489–497.

(64) Yang, G.; Meir, N.; Raanan, D.; Oron, D. Band Gap Engineering Improves the Effi-

ciency of Double Quantum Dot Upconversion Nanocrystals. *Advanced Functional Materials* **2019**, *29*, 1900755.

(65) Khan, A. H.; Bertrand, G. H.; Teitelboim, A.; Sekhar M, C.; Polovitsyn, A.; Brescia, R.; Planelles, J.; Climente, J. I.; Oron, D.; Moreels, I. CdSe/CdS/CdTe Core/Barrier/Crown Nanoplatelets: Synthesis, Optoelectronic Properties, and Multiphoton Fluorescence Upconversion. *ACS nano* **2020**, *14*, 4206–4215.

(66) Yang, G.; Kazes, M.; Raanan, D.; Oron, D. Bright Near-Infrared to Visible Upconversion Double Quantum Dots Based on a Type-II/Type-I Heterostructure. *ACS Photonics* **2021**, *8*, 1909–1916.

(67) Bailey, R. E.; Nie, S. Alloyed Semiconductor Quantum Dots: Tuning the Optical Properties without Changing the Particle Size. *J. Am. Chem. Soc.* **2003**, *125*, 7100–7106.

(68) Wang, F.; Reece, P. J.; Paiman, S.; Gao, Q.; Tan, H. H.; Jagadish, C. Nonlinear optical processes in optically trapped InP nanowires. *Nano Lett.* **2011**, *11*, 4149–4153.

(69) Sanatinia, R.; Swillo, M.; Anand, S. Surface second-harmonic generation from vertical GaP nanopillars. *Nano Lett.* **2012**, *12*, 820–826.

(70) Fedorov, V. V.; Bolshakov, A.; Sergaeva, O.; Neplokh, V.; Markina, D.; Bruyere, S.; Saerens, G.; Petrov, M. I.; Grange, R.; Timofeeva, M.; Makarov, S. V.; Mukhin, I. S. Gallium Phosphide Nanowires in a Free-Standing, Flexible, and Semitransparent Membrane for Large-Scale Infrared-to-Visible Light Conversion. *ACS Nano* **2020**, *14*, 10624–10632.

(71) Xu, L.; Saerens, G.; Timofeeva, M.; Smirnova, D. A.; Volkovskaya, I.; Lysevych, M.; Camacho-Morales, R.; Cai, M.; Zangeneh Kamali, K.; Huang, L.; Karouta, F.; Tan, H. H.; Jagadish, C.; Miroshnichenko, A. E.; Grange, R.; Neshev, D. N.; Rahmani, M. Forward and Backward Switching of Nonlinear Unidirectional Emission from GaAs Nanoantennas. *ACS Nano* **2020**, *14*, 1379–1389.

(72) Dobrovolsky, A.; Sukrittanon, S.; Kuang, Y.; Tu, C. W.; Chen, W. M.; Buyanova, I. A. Energy upconversion in GaP/GaNP core/shell nanowires for enhanced near-infrared light harvesting. *Small* **2014**, *10*, 4403–4408.

(73) Cheriton, R.; Sadaf, S. M.; Robichaud, L.; Krich, J. J.; Mi, Z.; Hinzer, K. Two-photon photocurrent in InGaN/GaN nanowire intermediate band solar cells. *Communications Materials* **2020**, *1*, 1–7.

(74) Jansson, M.; Ishikawa, F.; Chen, W. M.; Buyanova, I. A. Designing Semiconductor Nanowires for Efficient Photon Upconversion via Heterostructure Engineering. *ACS Nano* **2022**, *16*, 12666–12676.

(75) De Roo, J. Chemical Considerations for Colloidal Nanocrystal Synthesis †. **2022**, *34*, 5766–5779.

(76) Ghosh, Y.; Mangum, B. D.; Casson, J. L.; Williams, D. J.; Htoon, H.; Hollingsworth, J. A. New insights into the complexities of shell growth and the strong influence of particle volume in nonblinking "giant" core/shell nanocrystal quantum dots. *Journal of the American Chemical Society* **2012**, *134*, 9634–9643.

(77) Hamachi, L. S.; Yang, H.; Jen-La Plante, I.; Saenz, N.; Qian, K.; Campos, M. P.; Cleveland, G. T.; Rreza, I.; Oza, A.; Walravens, W.; Chan, E. M.; Hens, Z.; Crowther, A. C.; Owen, J. S. Precursor reaction kinetics control compositional grading and size of CdSe1-: XSx nanocrystal heterostructures. *Chemical Science* **2019**, *10*, 6539–6552.

(78) Drake, G. A.; Keating, L. P.; Shim, M. Design Principles of Colloidal Nanorod Heterostructures. **2022**,

(79) Welsch, T. A.; Cleveland, J. M.; Chase, D. B.; Doty, M. F. Separating the Effects of Nonorthogonal Variables on the Hot-Injection Synthesis of Core/Thick-Shell ("Giant") CdTe/CdS Quantum Dots. *Chemistry of Materials* **2022**, *34*, 10721–10731.

Accepted Manuscript
Version of Record at: https://doi.org/10.1021/acsaom.3c00067

TOC Graphic